J. Fluid Mech. (1996), *vol.* 321, *pp.* 87–120
Copyright © 1996 Cambridge University Press

Interaction of capillary waves with longer waves. Part 1. General theory and specific applications to waves in one dimension

By KENNETH M. WATSON[1] AND STEVEN B. BUCHSBAUM[2]

[1] Marine Physical Laboratory, Scripps Institution of Oceanography, University of California at San Diego, CA 92093-0213, USA

[2] Science Applications International Corporation, 10260 Campus Point Drive, San Diego, CA 92121, USA

(Received 21 February 1995 and in revised form 27 February 1996)

A Hamiltonian formulation is used to investigate irrotational capillary wave dynamics. Dissipation is accounted for by putting the wave system in contact with a 'heat bath'. The generation of short waves by longer waves is studied. It is found that millimetre-wavelength waves tend to be created on the forward face of a steep longer wave, while centimetre waves tend to form near the crest. Generation of capillary waves by wind waves is investigated. The results are compared with predictions of the Hasselmann transport equation. It is found that off-resonance interactions lead to significant corrections to the transport theory. The relative importance of three-wave and four-wave interactions is studied, as well as the role of triad resonances. For the capillary phenomena studied here, the four-wave terms in most cases lead to quantitative, but not qualitative, corrections to the three-wave only calculations. However, restricting interactions to the neighbourhood of triad resonances can give quite erroneous results. Use of a canonical transformation to pseudo-wave variables can greatly reduce numerical computation times.

1. Introduction

Capillary wave dynamics are of importance for remote sensing (see, for example, Donelan & Pierson 1987 and Apel 1994) and for the mechanism of longer wave breaking (see, for example, Longuet-Higgins 1992; Longuet-Higgins & Cleaver 1994; Longuet-Higgins, Cleaver & Fox 1994; Duncan *et al.* 1994). Recent experiments of Jähne & Riemer (1990) and Klinke & Jähne (1992) have studied the spectrum of short gravity–capillary waves for wavelengths in the range from less than 0.5 to about 20 cm. An important conclusion from these observations is that nonlinear interactions with longer waves provide an important mechanism for capillary wave generation. Other experiments by Cox (1958), Zhang & Cox (1994), Zhang (1995), and Miller, Shemdin & Longuet-Higgins (1992) have lead to similar conclusions. A spectral model based on these observations has been proposed by Apel (1994).

Theoretical analyses of capillary wave generation have been given by Longuet-Higgins (1963, 1995) and, using the Hasselmann (1968) transport equation, by Valenzuela & Liang (1972), Holliday (1977), van Gastel (1987*a*, *b*), and Watson & McBride (1993). Strong interactions lead to short energy exchange times – of the order of fractions of a second, in sharp contrast to those for longer wavelengths where wave groups may propagate for kilometres to hundreds of kilometres.

In the analyses cited above, the nonlinear equations were truncated at the order of *three-wave interactions*. The Hasselmann transport equation is obtained from these truncated equations by the approximations of *cumulant discard*, which neglects correlation effects from different spectral regions, and *weak interaction theory*, which restricts interactions to *triad resonances*.

In the present paper we have three principal objectives. The first is to obtain numerical solutions of the truncated three-wave equations, from which the Hasselmann (1968) model is derived. This will permit an assessment of the accuracy of this model. Our second objective is to investigate the mechanisms of capillary wave generation – for example, the position where capillary waves are formed relative to the longer wave profile. Our third objective is to include the four-wave term in the equations of motion in order to see the relative importance of the three- and four-wave terms. In addition to addressing these objectives, we shall describe a technique, using canonical transformation theory, that can significantly reduce the computational load for capillary wave calculations.

Our formulation of wave dynamics begins with a Hamiltonian formulation which assumes inviscid irrotational flow. An extension of this model is also used which incorporates wind input and viscous damping by supposing the wave system to be in contact with a 'heat bath'.

The formulation of surface wave dynamics in terms of a Hamiltonian has been given by Zakharov (1968), Miles (1977), and Milder (1990). This work is reviewed and adapted for our present analysis in §2. By considering the wave system to be bounded by a rectangular box, the Hamiltonian is expressed in terms of discrete canonical variables and provides first-order evolution equations in time. The observations of Jähne and his collaborators imply that the capillary spectrum does not extend to wavelengths much less than $\lambda = \frac{1}{2}$ to $\frac{2}{3}$ cm. Termination of the variable set in this wavelength regime means that the Hamiltonian has a finite set of degrees of freedom.

Our applications in §3 begin with a study of the *Wilton #2 triad* and some generalizations of this (Wilton 1915). We next investigate the radiation of parasitic capillary waves from a longer wave (Ebuchi, Kawamura & Toba 1987; Perlin, Liu & Ting 1993; Longuet-Higgins 1995). Our final application is to the generation of capillary waves from a Donelan–Pierson (1987) wind wave spectrum. Here we compare the generation process and rates with those obtained by Watson & McBride (1993) using the Hasselmann model.

In §4 we extend the theory by applying a canonical transformation to remove three-wave interaction terms from the Hamiltonian which do not involve triad resonances. The Lie method of Creamer *et al.* (1989) is used here. Since the domain of triad resonances is limited to relatively short wavelengths, we can remove from the calculation all the longer waves. A very substantial reduction in computing time can thus be achieved. After integrating the dynamic equations, the inverse canonical transformation restores effects of the longer waves. Applications of the canonical transformation technique are given in §5.

The formal theory here will be developed for waves in two surface dimensions; however, most of the applications described in this paper will be to waves in a single surface dimension. Part 2 will address in more detail wave phenomena in two surface dimensions.

2. Hamiltonian dynamics

In this section we review the Hamiltonian formulation of surface wave dynamics and put this into a form convenient for our calculations.

Our 'ocean' is confined to a rectangular box of dimensions X and Y with area $\mathscr{A}_0 = XY$. A rectangular coordinate system is used with the plane of the undisturbed water surface at $z = 0$ and points above this surface at $z > 0$. A horizontal vector in the surface $z = 0$ is written as $\boldsymbol{x} = (x, y)$. The flow is assumed to be irrotational and inviscid. The velocity potential is $\Phi(\boldsymbol{x}, z)$. The vertical displacement of the surface at $\boldsymbol{x}$ is $\zeta(\boldsymbol{x})$. The velocity potential evaluated at the water surface is

$$\phi(\boldsymbol{x}) \equiv \Phi(\boldsymbol{x}, \zeta(\boldsymbol{x})). \tag{2.1}$$

The vertical and horizontal components of velocity at the surface $z = \zeta$ are

$$w = \frac{\partial \Phi}{\partial t} \equiv \hat{D}\phi, \quad \boldsymbol{u} = \nabla \Phi_{z=\zeta} = \nabla\phi - w\nabla\zeta. \tag{2.2}$$

The operator ∇ here is the gradient operator acting in the (x, y)-plane. The Hamiltonian is the energy of the wave system (see Zakharov 1968; Miles 1977). Using the notation of Milder (1990) and normalizing energy and action to unit water density, we write this as

$$\mathscr{H} = \frac{1}{2}\int [\phi \hat{K}\phi + g\zeta^2 + 2\tau(1 + (\nabla\zeta)^2)^{1/2} - 2\tau]\,\mathrm{d}\boldsymbol{x}. \tag{2.3}$$

Here g is the acceleration due to gravity and

$$\tau = 7.5 \times 10^{-5}\ \mathrm{m^3\ s^{-2}}$$

represents a nominal value for the surface tension parameter. Following Milder (1990) we have

$$\hat{K} \equiv [1 + (\nabla\zeta)^2]\,\hat{D} - \nabla\zeta \cdot \nabla.$$

The field quantities ϕ and ζ represent canonical variables and the Hamiltonian equations of motion are

$$\frac{\partial \zeta}{\partial t} = \frac{\delta \mathscr{H}}{\delta \phi}, \quad \frac{\partial \phi}{\partial t} = -\frac{\delta \mathscr{H}}{\delta \zeta}. \tag{2.4}$$

It is convenient to Fourier expand the field amplitudes in the area $\mathscr{A}_0$:

$$\left.\begin{aligned} \phi(\boldsymbol{x}) &= \sum_{\boldsymbol{k}} [V_k/(2\mathscr{A}_0)]^{1/2} [b_{\boldsymbol{k}} \mathrm{e}^{\mathrm{i}\boldsymbol{k}\cdot\boldsymbol{x}} + \text{c.c.}], \\ \zeta(\boldsymbol{x}) &= i\sum_{\boldsymbol{k}} [1/(2\mathscr{A}_0 V_k)]^{1/2} [b_{\boldsymbol{k}} \mathrm{e}^{\mathrm{i}\boldsymbol{k}\cdot\boldsymbol{x}} - \text{c.c.}]. \end{aligned}\right\} \tag{2.5}$$

We have written

$$V_k = \omega_k / k \tag{2.6}$$

as the phase velocity for a linear wave having wavenumber k and angular frequency

$$\omega_k = [k(g + \tau k^2)]^{1/2}. \tag{2.7}$$

The discrete wavenumber vectors $\boldsymbol{k}$ are of the form

$$k_x = k_{0x} n_x, \quad k_{0x} \equiv \frac{2\pi}{X}, \quad k_y = k_{0y} n_y, \quad k_{0y} \equiv \frac{2\pi}{Y}, \quad n_x, n_y \text{ integer}. \tag{2.8}$$

The wavenumbers here will be restricted to the range

$$|k_x| < k_{cx}, \quad |k_y| < k_{cy}. \tag{2.9}$$

which will be specified in detail later. We thus have a finite set D of wavenumbers.

Canonical action-angle variables J_k and θ_k are related to the Fourier amplitudes in (2.5):

$$b_k = J_k^{1/2} e^{-i\theta_k}. \tag{2.10}$$

The b are 'action amplitude' variables. Poisson bracket relations for the action amplitude variables are

$$\{b_k, b_{k'}\} \equiv \sum_p \left[\frac{\partial b_k}{\partial \theta_p}\frac{\partial b_{k'}}{\partial J_p} - \frac{\partial b_k}{\partial J_p}\frac{\partial b_{k'}}{\partial \theta_p}\right] = 0, \quad \{b_k, b_k^*\} = -i\delta_{k-k'}. \tag{2.11}$$

For functions G and H of b we may use an alternative form for the Poisson bracket,

$$\{G(\boldsymbol{b}), H(\boldsymbol{b})\} = -i\sum_p \left[\frac{\partial G}{\partial b_p}\frac{\partial H}{\partial b_p^*} - \frac{\partial G}{\partial b_p^*}\frac{\partial H}{\partial b_p}\right]. \tag{2.12}$$

Hamilton's equations of motion can be expressed as

$$\dot{J}_k = \{J_k, \mathscr{H}\} = -\frac{\partial \mathscr{H}}{\partial \theta_k}, \quad \dot{\theta}_k = \{\theta_k, \mathscr{H}\} = \frac{\partial \mathscr{H}}{\partial J_k}, \tag{2.13}$$

or

$$\dot{b}_k = \{b_k, \mathscr{H}\}. \tag{2.14}$$

Following Milder's (1990) prescription, we expand the Hamiltonian in ascending orders of the field variables:

$$\mathscr{H}(J, \theta) = \mathscr{H}_0(J) + \epsilon\mathscr{H}_1(J, \theta) + \epsilon^2\mathscr{H}_2(J, \theta) + \ldots, \tag{2.15}$$

where ϵ is a formal expansion parameter which will later be set equal to unity. Expressions for the terms above, in terms of ϕ and ζ, have been given by Milder (1990) and Watson & McBride (1993). Expressed in terms of $\boldsymbol{J}$, θ these are

$$\mathscr{H}_0 = \sum_k \omega_k J_k,$$

$$\mathscr{H}_1 = -\sum_{k,l,m} \{\tfrac{1}{3}\delta_{k+l+m} h(\boldsymbol{k}, \boldsymbol{l}, \boldsymbol{m}) \sin(\theta_k + \theta_l + \theta_m) + \delta_{k-l-m}\Gamma(\boldsymbol{k}, \boldsymbol{l}, \boldsymbol{m}) \sin(\theta_k - \theta_l - \theta_m)\}\left[\frac{J_k J_l J_m}{8\mathscr{A}_0 V_k V_l V_m}\right]^{1/2}, \tag{2.16}$$

where

$$\left.\begin{aligned}\Gamma(\boldsymbol{k}, \boldsymbol{l}, \boldsymbol{m}) &= \omega_k\omega_l(\hat{\boldsymbol{l}}\cdot\hat{\boldsymbol{k}} - 1) + \omega_k\omega_m(\hat{\boldsymbol{m}}\cdot\hat{\boldsymbol{k}} - 1) + \omega_l\omega_m(\hat{\boldsymbol{l}}\cdot\hat{\boldsymbol{m}} + 1),\\ h(\boldsymbol{k}, \boldsymbol{l}, \boldsymbol{m}) &= \omega_k\omega_l(\hat{\boldsymbol{k}}\cdot\hat{\boldsymbol{l}} + 1) + \omega_k\omega_m(\hat{\boldsymbol{k}}\cdot\hat{\boldsymbol{m}} + 1) + \omega_l\omega_m(\hat{\boldsymbol{l}}\cdot\hat{\boldsymbol{m}} + 1),\end{aligned}\right\} \tag{2.17}$$

and

$$\mathscr{H}_2 = -\frac{1}{4\mathscr{A}_0}\sum_{k,l,m,n}[J_k J_l J_m J_n]^{1/2}\left\{\delta_{k+l+m+n}\cos(\theta_k + \theta_l + \theta_m + \theta_n) \times\left[\left(\frac{V_k V_n}{V_l V_m}\right)^{1/2}(kn|\boldsymbol{m}+\boldsymbol{n}| - kn^2) + \tau/4\frac{\boldsymbol{k}\cdot\boldsymbol{l}\boldsymbol{m}\cdot\boldsymbol{n}}{(V_k V_l V_m V_n)^{1/2}}\right]\right.$$

$$+\delta_{k+l+m-n}\cos(\theta_k+\theta_l+\theta_m-\theta_n)\left[\left(\frac{V_k V_n}{V_l V_m}\right)^{1/2}(kn|\boldsymbol{m}-\boldsymbol{n}|+kn|\boldsymbol{k}+\boldsymbol{m}|-kn^2-k^2n)\right.$$

$$+\left(\frac{V_k V_m}{V_l V_n}\right)^{1/2}(km^2-km|\boldsymbol{m}-\boldsymbol{n}|)+\left(\frac{V_k V_l}{V_m V_n}\right)^{1/2}(kl^2-kl|\boldsymbol{m}+\boldsymbol{l}|)$$

$$\left.-\tau/4\frac{2\boldsymbol{k}\cdot\boldsymbol{l}\boldsymbol{m}\cdot\boldsymbol{n}+\boldsymbol{k}\cdot\boldsymbol{n}\boldsymbol{l}\cdot\boldsymbol{m}+\boldsymbol{k}\cdot\boldsymbol{m}\boldsymbol{l}\cdot\boldsymbol{n}}{(V_k V_l V_m V_n)^{1/2}}\right]$$

$$+\delta_{k+l-m-n}\cos(\theta_k+\theta_l-\theta_m-\theta_n)\left[\left(\frac{V_k V_n}{V_l V_m}\right)^{1/2}(2kn^2-kn|\boldsymbol{l}-\boldsymbol{n}|\right.$$

$$-kn|\boldsymbol{m}+\boldsymbol{n}|)+\left(\frac{V_k V_l}{V_m V_n}\right)^{1/2}(kl|\boldsymbol{m}-\boldsymbol{l}|-kl^2)$$

$$\left.-\tau/4\frac{\boldsymbol{k}\cdot\boldsymbol{l}\boldsymbol{m}\cdot\boldsymbol{n}+\boldsymbol{k}\cdot\boldsymbol{m}\boldsymbol{l}\cdot\boldsymbol{n}+\boldsymbol{k}\cdot\boldsymbol{n}\boldsymbol{l}\cdot\boldsymbol{m}}{(V_k V_l V_m V_n)^{1/2}}\right]\Bigg\} \tag{2.18}$$

The expansion (2.15) of the Hamiltonian is ordinarily truncated after either the *three-wave* term $\mathscr{H}_1$ or the four wave term $\mathscr{H}_2$. Since the equations are nonlinear, each of these terms actually describes three-, four-, five-, ... wave interactions. The notation used is convenient, since it represents their lowest-order interactions.

To account for viscous damping of the waves we imagine our wave system to be in contact with a *heat bath* with which energy can be exchanged. Viscous damping and/or wind input energy may thus be phenomenologically incorporated into our equations in a manner consistent with the Hamiltonian description. This is described in Appendix A.

The equations of motion may readily be obtained using (2.14). Dimensionless wave slope amplitudes $a_{\boldsymbol{k}}$ are more convenient for computation than the action amplitudes $b_{\boldsymbol{k}}$. These are related by the equation

$$b_k = -\mathrm{i}(\mathscr{A}_0 V_k/2)^{1/2} a_k \mathrm{e}^{-\mathrm{i}\omega_k t}/k. \tag{2.19}$$

The vertical displacement of the surface, expressed in terms of these amplitudes, is

$$\zeta(\boldsymbol{x}, t) = \sum_{\boldsymbol{k}} 1/(2k)[a_{\boldsymbol{k}} \mathrm{e}^{\mathrm{i}(\boldsymbol{k}\cdot\boldsymbol{x}-\omega_k t)} + \text{c.c.}]. \tag{2.20}$$

Expressed in terms of the slope amplitudes, the equations of motion are

$$\dot{a}_{\boldsymbol{k}} + \epsilon_1[\beta a_{\boldsymbol{k}}] = \epsilon_3 T_3(\boldsymbol{a}; \boldsymbol{k}) + \epsilon_4 T_4(\boldsymbol{a}; \boldsymbol{k}), \tag{2.21}$$

where we have truncated after the four-wave term. Here

$$T_3(\boldsymbol{a}; \boldsymbol{k}) = -\frac{\mathrm{i}}{8V_k}\sum_{l,p}\frac{k}{lp}\{\delta_{\boldsymbol{k}-\boldsymbol{l}-\boldsymbol{p}}\Gamma(\boldsymbol{k}, \boldsymbol{p}, \boldsymbol{l})\, a_l a_p \mathrm{e}^{\mathrm{i}(\omega_k-\omega_l-\omega_p)t}$$

$$+2\delta_{\boldsymbol{k}+\boldsymbol{l}-\boldsymbol{p}}\Gamma(\boldsymbol{p}, \boldsymbol{k}, \boldsymbol{l})\, a_p a_l^* \mathrm{e}^{\mathrm{i}(\omega_k+\omega_l-\omega_p)t} + \delta_{\boldsymbol{k}+\boldsymbol{l}+\boldsymbol{p}} h(\boldsymbol{l}, \boldsymbol{p}, \boldsymbol{k})\, a_l^* a_p^* \mathrm{e}^{\mathrm{i}(\omega_k+\omega_l+\omega_p)t}. \tag{2.22}$$

The expression for T_4 is of third order in the $\boldsymbol{a}$ and is rather lengthy so will not be given explicitly here. The quantity β describes viscous damping,

$$\beta = 2\nu k^2, \tag{2.23}$$

where ν is the kinematic viscosity, given here a nominal value of 1.3×10^{-6} m^2 s^{-1}. The coefficients ϵ_1, ϵ_3, ϵ_4 in (2.21) are each taken to be zero or unity, depending upon whether we wish to keep the corresponding term in our calculations.

The spectrum of action density $F(\boldsymbol{k})$ is obtained from the relations

$$J_k/\mathscr{A}_0 = \Delta^2 K F(\boldsymbol{k}), \tag{2.24}$$

where J_k is the wave action introduced in (2.10) and

$$\Delta^2 K = \left(\frac{2\pi}{X}\right)\left(\frac{2\pi}{Y}\right). \tag{2.25}$$

For closely spaced Fourier wavenumbers we can take the continuum limit of (2.24):

$$\sum_{\boldsymbol{k}} J_k/\mathscr{A}_0 = \int \mathrm{d}\boldsymbol{k}\, F(\boldsymbol{k}).$$

The spectrum of vertical displacement of the surface is

$$\Psi(\boldsymbol{k}) = F(\boldsymbol{k})/V_k. \tag{2.26}$$

For our applications it will be convenient to consider a grid that is imbedded in the area $\mathscr{A}_0$. We suppose this grid to have dimensions S_x and S_y, where

$$X = J_x S_x, \quad Y = J_y, S_y, \tag{2.27}$$

and J_x and J_y are positive integers. Wavenumbers in this grid we write as

$$\left.\begin{aligned} K_x &= k_{sx}(n_0 + n_x), \quad n_x = 1, 2, \ldots, M_x, \\ K_y &= k_{sy} n_y, \quad n_y = -M_y, \ldots, 0, \ldots, M_y, \end{aligned}\right\} \tag{2.28}$$

Here

$$k_{sx} = \frac{2\pi}{S_x}, \quad k_{sy} = \frac{2\pi}{S_y}, \tag{2.29}$$

and n_0, M_x, M_y are positive integers to be chosen as appropriate for specific calculations. Our wavenumber restriction in (2.28) implies that the principal direction of propagation is the positive direction along the x-axis.

As noted, the wavenumbers (2.8) form a finite set D. The subset (2.28) form a set D_S. Wavenumbers in D, but not in D_S, are said to belong to the set $D_{\bar{S}}$. The relations (2.28) imply that if we set

$$a_{\boldsymbol{k}} = 0, \quad t = 0, \quad \boldsymbol{k} \in D_{\bar{S}},$$

then

$$a_{\boldsymbol{k}}(t) = 0, \quad \text{all times}, \quad \boldsymbol{k} \in D_{\bar{S}}. \tag{2.30}$$

This follows from the δ-function restrictions on wavenumber triads and quartets in (2.21): for example,

$$\delta_{\boldsymbol{k} \pm \boldsymbol{L} - \boldsymbol{P}} = 0 \quad \text{when} \quad \boldsymbol{L}, \boldsymbol{P} \in D_S \quad \text{and} \quad \boldsymbol{k} \in D_{\bar{S}},$$

etc. Because of (2.30) may thus ignore the set $D_{\bar{S}}$ and integrate (2.21) only for wavenumbers in the set D_S. These waves will of course be periodic in the larger area $\mathscr{A}_0$. This results from the homogeneity of the Hamiltonian within this larger area.

The equations (2.21) for the set D_S now have the form

$$\dot{a}_{\boldsymbol{K}} + \epsilon_1[\beta a_{\boldsymbol{K}}] = \epsilon_3 T_3(\boldsymbol{a}; \boldsymbol{K}) + \epsilon_4 T_4(\boldsymbol{a}; \boldsymbol{K}), \tag{2.31}$$

where

$$T_3(\boldsymbol{a}; \boldsymbol{K}) = -\frac{\mathrm{i}}{8V_K} \sum_{\boldsymbol{L}, \boldsymbol{P}} \frac{K}{LP} \{\delta_{\boldsymbol{K}-\boldsymbol{L}-\boldsymbol{P}} \Gamma(\boldsymbol{K}, \boldsymbol{P}, \boldsymbol{L})\, a_{\boldsymbol{L}}\, a_{\boldsymbol{P}}\, \mathrm{e}^{\mathrm{i}(\omega_K - \omega_L - \omega_P)t}$$
$$+ 2\delta_{\boldsymbol{K}+\boldsymbol{L}-\boldsymbol{P}} \Gamma(\boldsymbol{P}, \boldsymbol{K}, \boldsymbol{L})\, a_{\boldsymbol{P}} a_{\boldsymbol{L}}^*\, \mathrm{e}^{\mathrm{i}(\omega_K + \omega_L - \omega_P)t}\}, \quad \boldsymbol{K}, \boldsymbol{L}, \boldsymbol{P} \in D_S, \tag{2.32}$$

with a corresponding expression for T_4. Because of the restriction to $K_x, L_x, P_x > 0$, the third term in (2.22) vanishes. A similar modification is made in the four-wave term T_4. Because of (2.30) we can assume that all modes in $D_{\bar{S}}$ have zero amplitudes.

The point of the above choice of a computational grid will be seen in §4. By means of a canonical transformation we can remove interactions from (2.32) not involving a triad *resonance*. The inverse canonical transformation generates numerical values for those mode amplitudes in $D_{\bar{S}}$.

To calculate the wave spectrum in the grid (2.28) we replace (2.25) by

$$\Delta^2 K = \left(\frac{2\pi}{S_x}\right)\left(\frac{2\pi}{S_y}\right). \tag{2.33}$$

For applications in one surface dimension we write, as an approximate model,

$$\Delta^2 K = 2K\Delta K\Delta\theta, \quad \Delta K = \left(\frac{2\pi}{S_x}\right), \quad \Delta\theta = \pi/4. \tag{2.34}$$

The dimensionless 'saturation' spectrum is, in one or two dimensions,

$$B(\boldsymbol{K}) \equiv B(k, \theta_K) = K^4 \Psi(\boldsymbol{K}), \tag{2.35}$$

where θ_K describes the direction of $\boldsymbol{K}$ with respect to the x-axis (for applications in one dimension, we set $\theta_K = 0$).

2.1. *Triad resonances*

A triad resonance occurs for those terms in (2.32) for which

$$f^{\pm} \equiv |\omega_K \pm \omega_L - \omega_P| < \epsilon_{res}. \tag{2.36}$$

In the Hasselman (1968) theory, for which the area $\mathscr{A}_0$ is presumed to be arbitrarily large, $\epsilon_{res} = 0$. Only those interactions in exact resonance are then of importance. In a theory such as ours with discrete wavenumbers, we might expect ϵ_{res} to represent some characteristic rate of energy transfer among modes.

In the four-wave term T_4 explicit time-dependent exponentials of the form

$$\exp[\mathrm{i}(\omega_k \pm \omega_l \pm \omega_m \pm \omega_p)\, t]$$

appear. A quartic resonance occurs when

$$|\omega_k \pm \omega_l \pm \omega_m \pm \omega_p| < \epsilon'_{res}, \tag{2.37}$$

where $\epsilon'_{res} = 0$ in the Hasselmann (1968) theory and is again (perhaps) determined by some evolution rate from (2.31).

Of primary interest for our study of capillary wave interactions is the term T_3 and the role of triad resonances in this term. For waves in one dimension, corresponding to $M_y = 0$ in (2.28), determining the location of triad resonances is straightforward†. We must first specify the high-wavenumber cut-off

$$k_{cx} = k_{sx} M_x \equiv 2\pi/\lambda_c. \tag{2.38}$$

As a consequence of this lower limit on wavelength, for a triad resonance to occur all three waves must lie in the domain D_R, a subset of the set D (2.8):

$$\lambda_r > \lambda > \lambda_c. \tag{2.39}$$

† The resonance domains in one and two dimensions were determined from contour plots in an (L_x, L_y)-plane of $\omega_K \pm \omega_L - \omega_P$, $\boldsymbol{P} = \boldsymbol{K} \pm \boldsymbol{L}$, for a given $\boldsymbol{K}$. For applications of the method of §4, a further test was made by printing the smallest values of $f^{\pm}$ outside the resonance domain.

λ_c (cm)	λ_r (cm)	S_x (cm)	n_0	Grid
2/3	10	10	0	G_1
2/3	10	20	1	G_2
1/2	12	12	0	G_3
1/4	26	To be specified	0	G_4

TABLE 1. Description of some resonance domains and related grids used for our calculations. Here λ_c is the short-wavelength cut-off, λ_r is the long-wavelength bound on the resonance domain, and S_x and n_0 are defined by (2.27) and (2.28)

In table 1 we show values for λ_c, λ_r and S_x to be used for our applications. For those calculations presented in §3 for waves in two dimensions, the specification of the resonance domains given in table 1 is adequate.

It is important to emphasize that all three members of the wave triad must lie in the domain D_R for a resonance to be possible. Wavenumbers not in D_R are said to be in the set $D_{\bar{R}}$. In §5 we shall extend the calculations to include the entire domain D.

2.2. *Computational details*

Integration of the coupled equations (2.31) was done using the Bulirsch–Stoer method, as described by Press *et al.* (1992). This proved to be a fast stable algorithm for these equations. The calculations presented here were done in double precision on a Power Macintosh computer (for a check, selected calculations were repeated, with an independently written code, on a Sun workstation). The complex slope amplitudes were printed to files at specified times over the duration of the integration. Also, at specified times, values for the spectrum B and the energy (value of the Hamiltonian) were printed to a file. The quantity B was printed in exponential format to three significant figures and the energy in exponential format to four significant figures.

With $\epsilon_1 = 0$ in (2.31) energy is conserved, which gave a useful check of numerical accuracy. When $\epsilon_1 = 1$, viscous damping led to energy decrease of up to 10% in our calculations.

Numerical calculations were started at time $t = 0$ in one of two ways: a specific file of initial amplitudes could be read; alternatively, a wind-wave spectrum could be generated using the Donelan–Pierson (1987) spectrum for the $|a_K|$, with a random number generator to give the phases. The set of input amplitudes was saved to a file. This permitted repeating calculations with a given set of input amplitudes.

To provide insight into the significance of triad resonances, a 'filter' was introduced into T_3 (2.32). This 'filter' drops from the summation in T_3 the first or the second term if

$$f^- > f_{lim} \quad \text{or} \quad f^+ > f_{lim}, \tag{2.40}$$

respectively, where $f^{\pm}$ is defined by (2.36) and f_{lim} is an adjustable parameter. The corresponding term is also dropped from the Hamiltonian term $\mathscr{H}_1$ (2.16) so the truncated equations remain a Hamiltonian system.

A similar 'filter' was introduced into $\mathscr{H}_2$ and T_4.

To investigate the significance of 'off-resonance' terms, f_{lim} was initially given a small value. The calculation was repeated with increasing values until no change was found in the values of $B(K)$, to the above-described printed accuracy, after the last time interval. (This proved to be a more stringent test than a visual inspection of plots of the wave displacement $\zeta(x, t)$ and/or wave slope.) We shall adopt the convention of referring to that f_{lim} at which no further change in B is found as giving an 'exact' result.

To check the accuracy of the four-wave term T_4, two calculations were made with $\epsilon_1 = 0$ and the results compared with similar previously published calculations. The first was of the Benjamin–Feir (1967) (Benjamin 1967) instability, comparison being with the simple model of Whitham (1974). The second calculation was of the propagation of the 'Feir soliton', studied by Cohen, Watson & West (1976).

3. Applications

In this section we describe several applications of the theory presented in §2.

3.1. *Wilton ripple instability*

The Wilton '$n = 2$' instability is represented by the resonant triad (Wilton 1915; Henderson & Hammack 1987):

$$k_a = k_b = \left(\frac{g}{2\tau}\right)^{1/2} = 258 \text{ m}^{-1}, \quad k_c = 2k_a. \tag{3.1}$$

We shall use grids G_1 and G_2 (see table 1), which slightly displace the triad wavenumbers to

$$k_a = k_b = 251.3 \text{ m}^{-1}, \quad k_c = 502.6 \text{ m}^{-1}. \tag{3.2}$$

The resulting resonance mismatch,

$$\Delta\omega_1 \equiv \omega_c - 2\omega_a = -0.6 \text{ s}^{-1}, \tag{3.3}$$

is not significant here. A related 'harmonic' triad has a wavenumber

$$k_d = k_a + k_c = 753.9 \text{ m}^{-1}, \quad \Delta\omega_2 \equiv \omega_d - \omega_c - \omega_a = 18.3 \text{ s}^{-1}. \tag{3.4}$$

McGoldrick (1965) has given a simple analytic solution for the amplitudes a_a, a_b, a_c for the special case that at time $t = 0$ $a_a = a_b$, $a_c = 0$. Because of the value of the mismatch (3.4) setting $f_{lim} = 10 \text{ s}^{-1}$ 'turned-off' the harmonic triad and permitted checking our calculations with McGoldrick's analytic expression.

Using grid G_2 with (see equation (2.31)) $\epsilon_1 = \epsilon_4 = 0$, $\epsilon_4 = 1$ and with initial amplitudes

$$a_a = 0.25, \quad a_c = 0.02, \quad a_d = 0.01, \quad \text{all other } a \text{ in the range } 10^{-4} \text{ to } 10^{-3},$$

we show in figure 1(*a*) the magnitudes of the slopes at $t = 0.1$ s. At later times mode d exceeds that of a or c, but at $t = 0.25$ s mode d slope is again the smallest of the three, etc. Slow growth of other modes is seen, as these 'feed off' modes a, c, d. This growth continues at later times. (For $f_{lim} = 10 \text{ s}^{-1}$, growth of these other modes was not seen.)

The effect of f_{lim} was investigated. For $f_{lim} = 20 \text{ s}^{-1}$, the growth of modes c and d is very similar to that of figure 1(*a*). The value $f_{lim} = 50 \text{ s}^{-1}$ gave an exact result (recall our definition of 'exact' in this context, given in the previous section). We note that the resonance mismatch (3.4) was not large enough to significantly limit the growth rate of mode d.

Figure 1(*b*) shows the same calculation as that of figure 1(*a*), except that now the four-wave term T_4 in (2.31) is included ($\epsilon_1 = 0$, $\epsilon_3 = \epsilon_4 = 1$). Continuing the calculation to $t = 0.25$ s showed modest effects of T_4. The choice $f_{lim} \geqslant 20 \text{ s}^{-1}$ in T_4 was satisfactory.

The Wilton instability was also studied in two dimensions using the grid G_1 with $S_x = S_y = 0.1$ m, $M_x = 15$, $M_y = 2$ (2.28). Excitation of modes for $|n_y| > 0$ was observed.

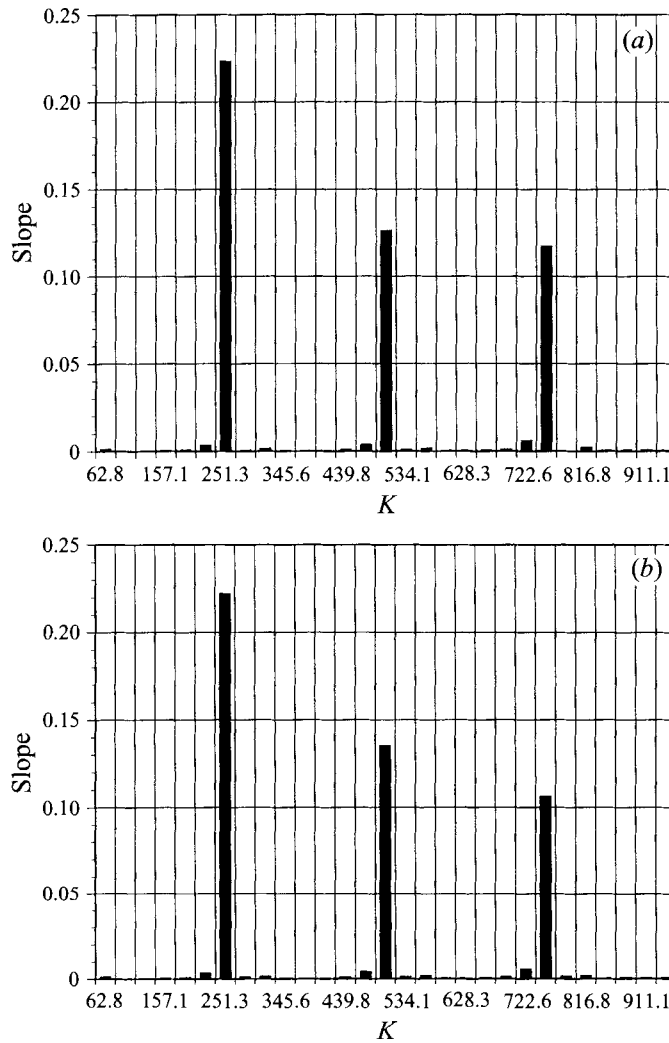

FIGURE 1. (*a*) Slope magnitudes for the Wilton triad amplitudes at $t = 0.1$ s. Modes and initial slope amplitudes are described by (3.1) and subsequent equations. (*b*) As (*a*) except that four-wave interactions have also been included.

We conclude that for the Wilton instability a value of $f_{lim} = 50\ \mathrm{s}^{-1}$ gave exact results. The increase of f_{lim} from 10 to 20 s^{-1} 'opened up' the *d*-wave channel. Increasing f_{lim} beyond 50 s^{-1} did not open up new channels for energy flow (by our criterion of exactness). If there were only the three modes *a*, *c*, *d*, we would find an oscillatory transfer of energy among these. Because of the other modes available, energy is fed to these from the *a*, *c*, *d* modes. A sufficiently large number of modes is required for spectral transport by this mechanism, but a resonance does not seem necessary.

3.2. *Radiation of parasitic capillary waves*

Generation of short capillary waves (wavelengths of a few mm) has been observed by Ebuchi *et al.* (1987), Perlin *et al.* (1993), and Zhang (1995). A physical theory for this has been given by Longuet-Higgins (1995), who chose a finite-amplitude Stokes wave as the radiating source.

In contrast to the model of Longuet-Higgins (1995), who considered a quasi-stationary state, we begin our calculation at $t = 0$ with a given Stokes wave and let the system evolve in time. We describe a sequence of Stokes waves of increasing slope (defined as the maximum value of $|\partial\zeta/\partial x|$). The parameters for these waves were chosen to match the regime of waves considered by Longuet-Higgins (1995).

For a Stokes wave slope of 0.2 or less no significant generation of millimetre-wavelength capillary waves was found.

For the calculation of figure 2 we start at $t = 0$ with a 10 cm wavelength Stokes wave of slope 0.25. We include dissipation ($\epsilon_1 = \epsilon_3 = 1$, $\epsilon_4 = 0$) and use the grid G_4 with $S_x = 10$ cm. In figure 2(*a*) we show as the heavy line the wave displacement ζ at $t = 0.3$ s.

To display wave slope in our work we use two filters, which pass waves only in the indicated bands:

$$\left.\begin{aligned} F_h&: \quad 0.25 \leqslant \lambda \leqslant 0.67 \text{ cm}, \\ F_m&: \quad 0.67 \leqslant \lambda \leqslant 2.5 \text{ cm}, \end{aligned}\right\} \tag{3.5}$$

The first filter gives the slope resulting from the Longuet-Higgins (1995) capillary waves. The waves passed by the second filter are of interest for some remote sensing applications.

The light curve in figure 2(*a*) represents wave slope $\partial\zeta/\partial x$ output from the filter F_h. Removing the dissipation term from (2.31) had very little effect at $t = 0.3$ s. This wave system is very similar to those calculated by Longuet-Higgins (1995), with waves of a few mm wavelength on the forward crest of the Stokes wave. In figure 2(*b*) we show the same wave at the same time as in figure 2(*a*), except that now we exhibit the slope output from filter F_m. Curve (i) represents the displacement ζ as seen in figure 2(*a*). Curve (ii) is the slope output from filter F_m. We note that in this band the slope is more centred under the wave crest.

For curve (iii) in figure 2(*b*) the calculation was repeated with a short-wave cut-off $\lambda_c = \frac{1}{2}$ cm and $S_x = 10$ cm. Curve (iii) represents the slope output from filter F_m, but displaced upward by 0.2. For curve (iv) the calculation was again repeated, but with a short-wave cut-off $\lambda_c = \frac{2}{3}$ cm and $S_x = 10$ cm, and representing the slope output from filter F_m, but displaced by 0.4.

Extending the numerical calculation to very short wavelengths considerably increases the computational burden. This is particularly the case if the long-wave limit λ_r is then increased to include the entire triad resonance domain. The implication of figure 2(*b*) is that we can obtain a fair description of the longer wave field without including the shortest waves in the calculation.

In figure 2(*c*) we show, again at $t = 0.3$ s, the result of superimposing at $t = 0$ the Stokes wave of figure 2(*a*) on a sine wave of 40 cm wavelength. (The canonical transformation technique to be described in §4 was used for this calculation.) For figure 2(*c*) the 40 cm sine wave was given a slope of 0.3. The heavy curve is displacement and the light curve is slope output from filter F_h. In addition to the vertical displacement of the Stokes wave, a significant distortion and wavelength shift due to strain are seen. The fine-scale surface roughness is also modified. When the 40 cm wave has a slope of 0.1 or less, the principal effect is just a linear superposition of the two wave systems.

Extending the calculation of figure 2 to $t = 2.0$ s does not greatly change the wave system. With dissipation 'turned off', the capillary wave field contained somewhat more noise.

For the calculations shown in figure 2 the minimum value of f_{lim} required for an exact result was 400 s^{-1}. This almost 10 times larger than the value needed for the

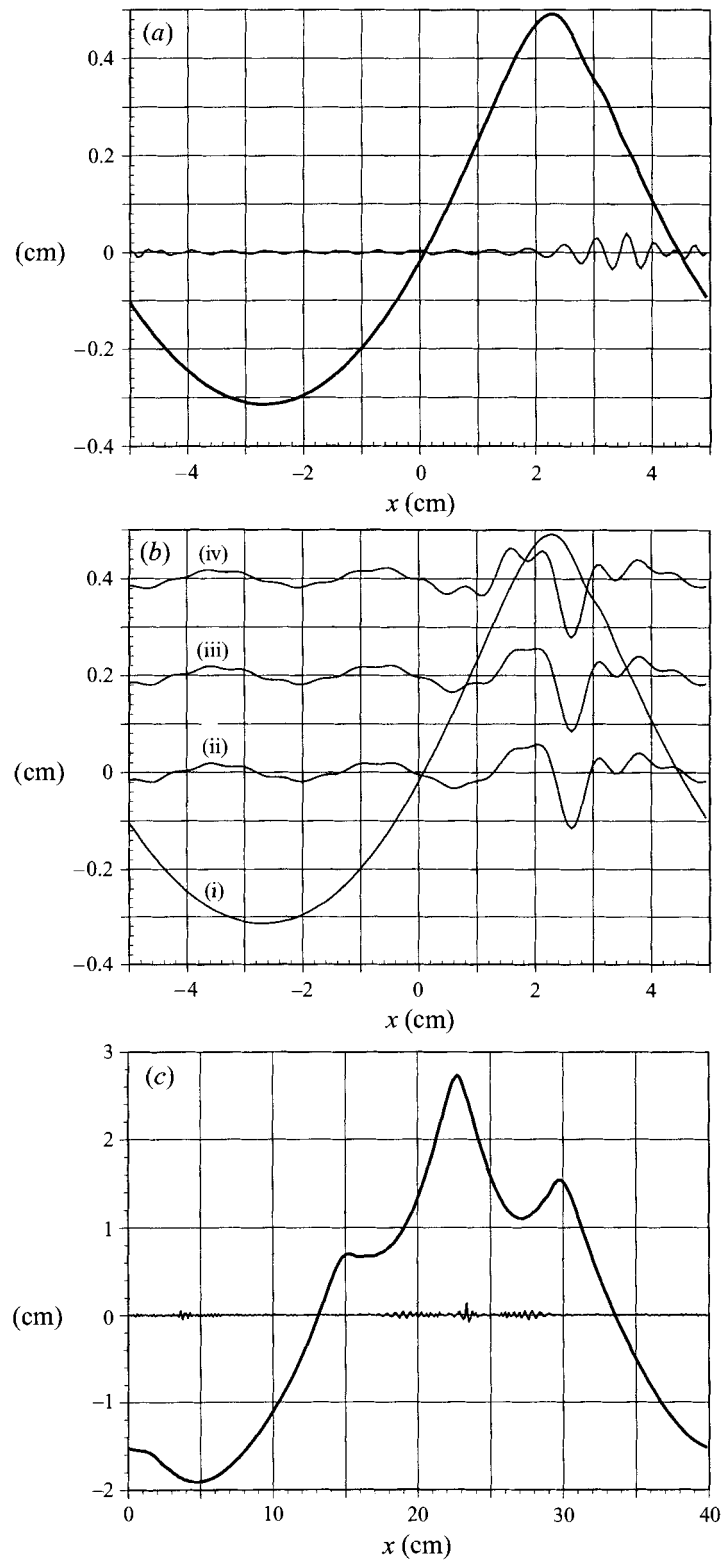

FIGURE 2(*a–c*). For caption see facing page.

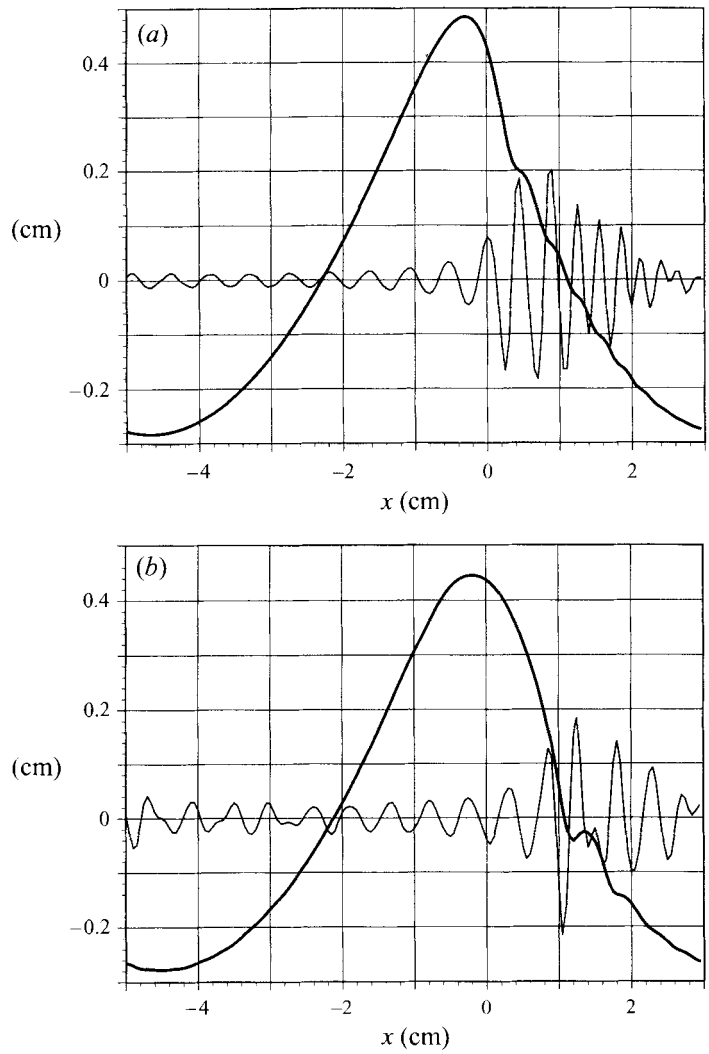

FIGURE 3. (*a*) Wave system at $t = 0.2$ s evolved without dissipation from an initial Stokes wave of 8 cm wavelength and slope 0.3. The light curve is F_h (3.5) filtered slope. (*b*) As (*a*) except that three- and four-wave interactions are included.

Wilton system. The larger value of f_{lim} needed here is presumably a result of phase locking, driving waves at rates far from their linear frequencies, and also from extension of the calculation to shorter higher-frequency waves.

For figure 3(*a*) we have started the calculation at $t = 0$ with the Longuet-Higgins Stokes wave of 8 cm wavelength, a slope of 0.3, and $S_x = 8$ cm. The results were calculated without dissipation ($\epsilon_1 = \epsilon_4 = 0$, $\epsilon_3 = 1$) and the time for the wave displayed in figure 3(*a*) is $t = 0.2$ s. The heavy curve is vertical displacement and the light curve

FIGURE 2. (*a*) Wave system at $t = 0.3$ s evolved with dissipation from an initial Stokes wave of 10 cm wavelength and slope 0.25. Heavy curve is surface displacement ζ and light curve is F_h filtered slope (3.5). (*b*) As (*a*) except that light curves represent slope output from filter F_m (3.5). Three slope curves are calculated with respective short-wave cut-offs of 0.25, 0.5, and 0.67 cm, as described in the text. The slope curve (iii) is displaced upward by 0.2, curve (iv) by 0.4. (*c*) Same Stokes wave as in (*a*), but superimposed on a 40 cm wavelength sine wave of slope 0.3.

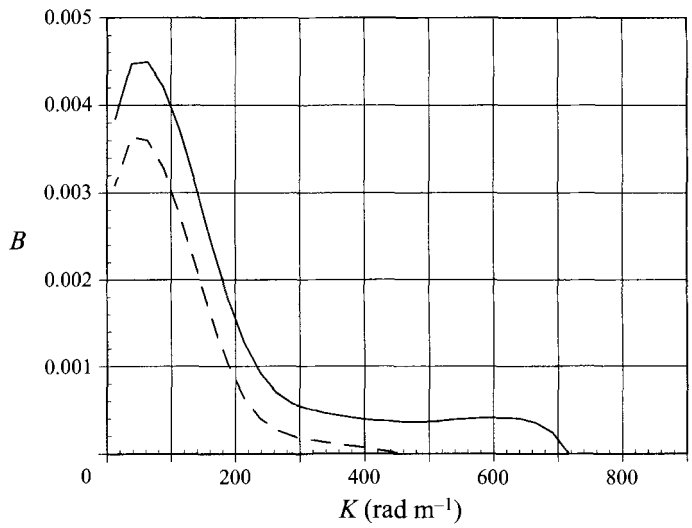

FIGURE 4. The Donelan–Pierson (1987) dimensionless saturation spectra for wind speeds of 4 m s^{-1} (dashed curve) and 6 m s^{-1} (solid curve).

is the F_h filtered slope. Figure 3(*b*) shows the same wave system at $t = 0.2$ s, but calculated with three- and four-wave interactions ($\epsilon_1 = 0$, $\epsilon_3 = \epsilon_4 = 1$). The four-wave interaction T_4 has increased the noise level of the rather simple Longuet-Higgins (1995) pattern arising from T_3. Although individual crests can be identified with those of figure 3(*a*), additional waves generated by T_4 appear to give rise to an interference pattern.

For the steep wave system of figure 3 a value $f_{lim} = 600$ s^{-1} was required for an exact result. (If dissipation had been included, $f_{lim} = 400$ s^{-1} would have been adequate.)

3.3. *Wind wave spectra*

As mentioned in the Introduction, calculations of capillary wave generation from a spectrum of longer wind waves have been published by Valenzuela & Liang (1972), Holliday (1977), van Gastel (1987*a*, *b*), and Watson & McBride (1993). These investigations have all used the Hasselmann (1968) radiative transport equation. In order to provide an assessment of the accuracy of the Hasselmann approximation, we shall repeat such calculations by integrating equations (2.31). We emphasize that the Hasselmann equation used by the above authors was derived from equations (2.31) with the four-wave term dropped ($\epsilon_4 = 0$).

For these calculations we generate an input file from the Donelan–Pierson (1987) spectrum for the magnitudes $|a_K|$. A random number generator is used to assign phases to these initial amplitudes. The input files are saved for re-use when we wish to compare different calculations (for example, the dependence on f_{lim}).

In figure 4 we show the Donelan–Pierson value of $B(K, 0)$, see (2.35), in the downwind direction for wind speeds of $U_{10} = 4$ and 6 m s^{-1}. The sharp cut-off at high wavenumbers is not observed (see, for example, Jähne & Riemer 1990 and Zhang 1995). The extension of the physical wave spectra is attributed to hydrodynamic generation of the shorter waves.

In figure 5(*a*) we show for a wind speed $U_{10} = 4$ m s^{-1} the saturation spectrum

FIGURE 5. (*a*) The satuation spectrum for $U_{10} = 4$ m s^{-1} with dissipation and at $t = 0.2$ s. (*b*) As (*a*) except that the calculation was extended to shorter wavelengths and the time is 1.6 s. (*c*) As (*a*) but calculated using three- and four-wave interactions.

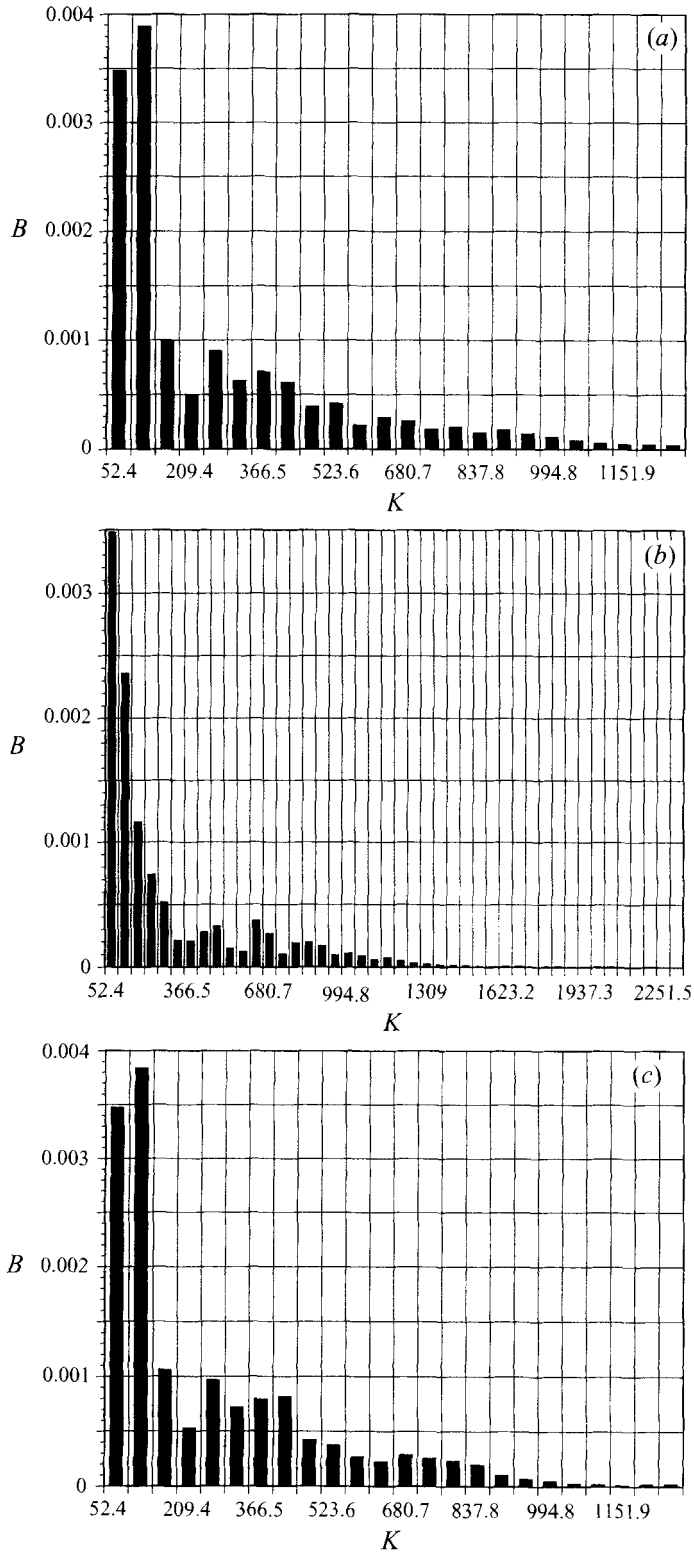

FIGURE 5(*a–c*). For caption see facing page.

$B(K, 0)$ from (2.35), using (2.34), at time $t = 0.2$ s. The grid G_3 (table 1) was used with $\lambda_c = \frac{1}{2}$ cm and including dissipation ($\epsilon_1 = \epsilon_3 = 1$, $\epsilon_4 = 0$). Five realizations of the wave field were averaged to obtain B. On comparing with figure 4 we note the extension of the spectrum to lower wavelengths, as anticipated. A characteristic time for generating the capillary waves is about 0.1 s. No dramatic change is found when the calculation is extended to 1.6 s. (A greater change would have been seen, however, if there were not dissipation.) For figure 5(*b*) the short-wave cut-off was extended to $\lambda_c = \frac{1}{4}$ cm (again, $\epsilon_1 = \epsilon_3 = 1$, $\epsilon_4 = 0$) and the time is 1.6 s. We see that there is negligible excitation for $K > 1300$ m^{-1}, consistent with the observations of Jähne & Riemer (1990).

For the calculations of figure 5(*a*, *b*) a value of $f_{lim} \geqslant 100$ s^{-1} was required in (2.40). A value this large implies that energy transfer occurs through channels not available in the Hasselmann (1968) theory.

For figure 5(*c*) the calculation of figure 5(*a*) was repeated with the same initial amplitudes, except that the four-wave interaction was included ($\epsilon_1 = \epsilon_3 = \epsilon_4 = 1$). The time is again 0.2 s. Figures 5(*a*) and 5(*c*) differ in detail, but the effect of T_4 is not dramatic.

Figure 6 shows the development of the wave spectrum in two surface dimensions and for a wind speed $U_{10} = 6$ m s^{-1}. The grid G_3 of table 1 was used, with $S_x = S_y = 12$ cm and including dissipation ($\epsilon_1 = \epsilon_3 = 1$, $\epsilon_4 = 0$). A value of $f_{lim} \geqslant 100$ s^{-1} was required for an exact calculation at $t = 1$ s. Five realizations were averaged to give the spectra shown in figure 6(*a*), where the time is 0.2 s. The time for figure 6(*b*) is also 0.2 s, but these data were calculated with $f_{lim} = 20$ s^{-1}. The dramatic effect of a larger f_{lim} in opening new channels for energy transport in wavenumber space is apparent.

We now describe a more detailed comparison with the Hasselmann model. The Hasselmann (1968) transport equation for three-wave interactions and inviscid flow is of the form

$$\frac{\mathrm{d}B(\boldsymbol{k})}{\mathrm{d}t} = a(\boldsymbol{k}) - b(\boldsymbol{k})\, B(\boldsymbol{k}). \tag{3.6}$$

Here $a(\boldsymbol{k})$ represents the rate of wave generation at $\boldsymbol{k}$ and $b(\boldsymbol{k})$ the rate of decay due to transport of energy away from $\boldsymbol{k}$ (there is no effect of viscosity in (3.6)). Since a and b are themselves dependent on $B(\boldsymbol{k})$, (3.6) is an integral equation. Most applications, such as that of Watson & McBride (1993), have evaluated a and b at time $t = 0$ when it is assumed that $B(\boldsymbol{k})$ is known. (Watson & McBride also used the Donelan–Pierson spectrum to provide B.)

To make a comparison with our present calculations we evaluate the dynamic generation rate as

$$\frac{\Delta B(\boldsymbol{k})}{\Delta t} \equiv \frac{B(\boldsymbol{k})_{t=T} - B(\boldsymbol{k})_{t=0}}{T}. \tag{3.7}$$

We identify (3.7) with the term $a(\boldsymbol{k})$ of (3.6) since initially there is little wave energy to lose from the capillary regime. For the evaluation of (3.7) the calculation was done in two surface dimensions with $\lambda_c = 0.5$ cm, $S_x = S_y = 10$ cm, no dissipation ($\epsilon_1 = \epsilon_4 = 0$, $\epsilon_3 = 1$, recall that (3.6) has no dissipation), and the time $T = 0.2$ s. These parameters match those of Watson & McBride (1993), where the triad resonance conditions in (3.6) restrict the interacting wavenumber domain to be the same as that chosen for integrating (2.31). Wind speeds of 4 and 6 m s^{-1} were considered and five realizations were averaged to give (3.7).

The values of $a(\boldsymbol{k})$ were taken from data of Watson & McBride (1993) (for a comparison, see figure 3 of their paper). The quantity a has sharp peaks at $k = 550$ m^{-1} for $U_{10} = 4$ m s^{-1} and at 700 m^{-1} for $U_{10} = 6$ m s^{-1}. Owing to the triad resonance

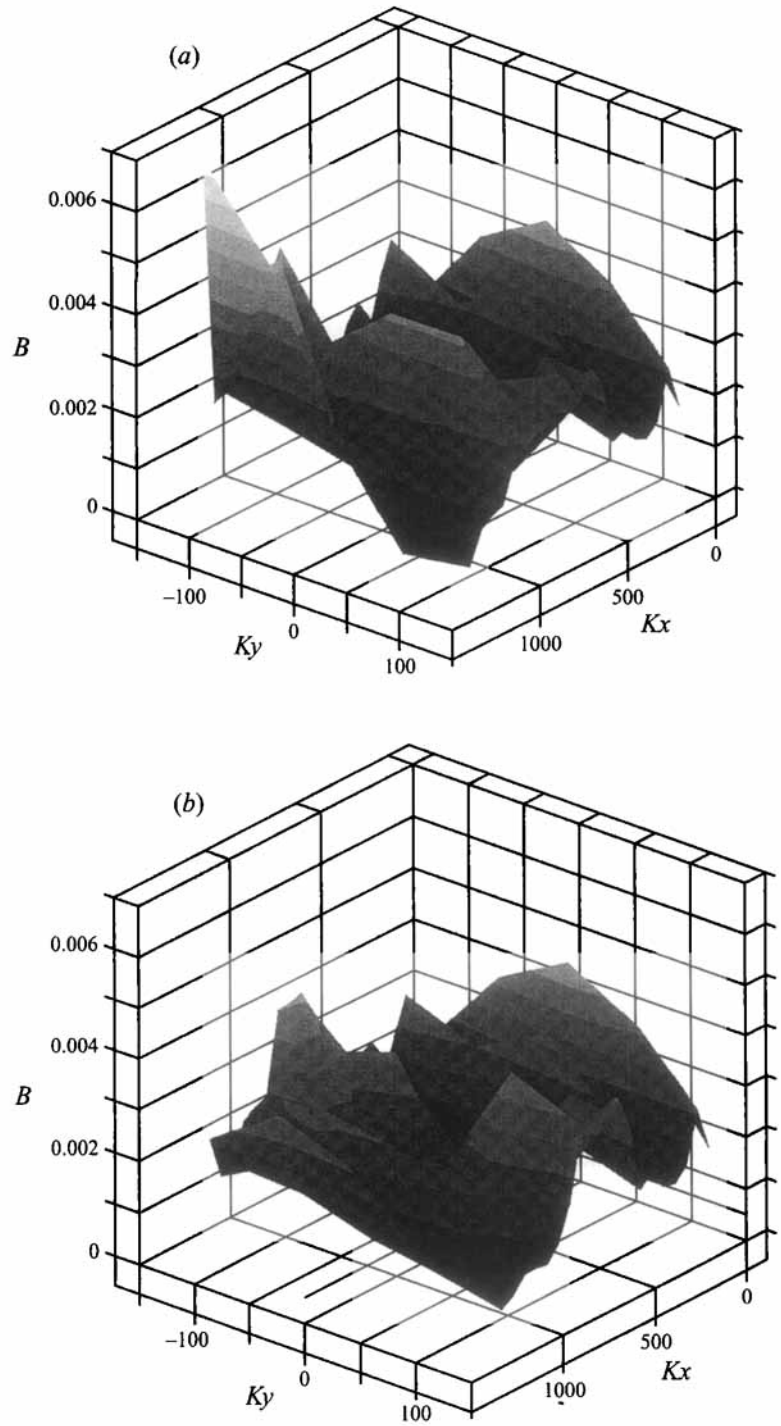

FIGURE 6. (*a*) Two-dimensional spectrum at $t = 0.2$ s for a wind speed of 6 m s^{-1}. (*b*) As (*a*) except that $f_{lim} = 20$ s^{-1}.

Wind speed ($m\ s^{-1}$)	Hasselmann rate ($W\ m^{-2}$)	Dynamic rate ($W\ m^{-2}$)	Three- and four-wave ($W\ m^{-2}$)
4	1.4×10^{-5}	1.0×10^{-4}	1.1×10^{-4}
6	3.8×10^{-4}	6.5×10^{-4}	—

TABLE 2. The energy transfer rates calculated by the Hasselmann theory and by the dynamic theory of this work. The rates are calculated using (3.6), (3.7), and (3.8) as described in §3. The three- and four-wave rate was calculated using both terms T_3 and T_4 in (2.31)

restriction little wave excitation occurs away from these peaks. In contrast to this, excitation described by (3.7) occurs over the broad wavelength interval $k > 250\ m^{-1}$. This can be seen on comparing figures (4) and 5(*a*).

We have calculated the linear wave energy transfer rate from (3.7) as

$$\dot{E}_D = \sum_{n_x, n_y} \rho_0 V_k^2 \dot{B}(\boldsymbol{k}) \Delta^2 K / k^3, \tag{3.8}$$

where ρ_0 is the density of water, $\Delta^2 K$ is defined by (2.33), and n_x, n_y describe discrete mode numbers. A similar expression was used to calculate the energy transfer rate $\dot{E}_H$ from (3.6). The resulting values are shown in table 2.

For $U_{10} = 4\ m\ s^{-1}$ the dynamic rate $\dot{E}_D$ is substantially larger than the Hasselmann rate $\dot{E}_H$. The Hasselmann rate is quite small at $4\ m\ s^{-1}$, presumably due to limited source waves matching the triad resonance condition. At $U_{10} = 6\ m\ s^{-1}$ the two rates are comparable. The difference in the two rates for both wind speeds seems associated with the excitation of a broad wavenumber band when the triad resonance condition does not apply.

For reference, we note that the total wave energy (as given by the value of the water density times the Hamiltonian/per unit area) is $1.46 \times 10^{-2}\ j\ m^{-2}$ at $U_{10} = 4\ m\ s^{-1}$ and $1.85 \times 10^{-2}\ j\ m^{-2}$ at $U_{10} = 6\ m\ s^{-1}$. From table 2 we see that only a very small fraction of the total wave energy has transferred to the capillary regime during the 0.2 s of the calculation.

The calculation at $U_{10} = 4\ m\ s^{-1}$ was repeated using the four-wave term T_4 in (2.31) ($\epsilon_1 = 0$, $\epsilon_3 = \epsilon_4 = 1$). The resulting energy transfer rate is shown in table 2. The four-wave terms are seen to lead to very little change in the rate.

4. Canonical transformation of variables

As the 'fetch' (i.e. the dimension of $\mathscr{A}_0$ along the x-axis) is increased, the number of modes required increases and the computational burden becomes greater. In the present section we attempt to mitigate this problem by use of a canonical transformation technique.

The objective of canonical transformation theory for nonlinear oscillators is to choose a new set of variables such that the nonlinear interaction terms in (2.31) vanish. This was achieved, for example, in the work of Creamer *et al.* (1989). Unfortunately, the presence of triad resonances precludes our doing this here in a straightforward fashion (an excellent review of this subject was given by Chirikov 1977). To work around the complication due to triad resonances, we follow the prescription of Meiss & Watson (1978) and Watson & McBride (1993), whose description of the canonical transformation we follow closely. Because we now require more detail than was given by these authors, we repeat some of their analysis.

We propose to make a transformation to new canonical action variables I_k, ϕ_k (for a discussion of canonical transformation theory see, for example, Goldstein 1969):

$$J_k, \theta_k \rightarrow I_k, \phi_k. \tag{4.1}$$

The transformed Hamiltonian will be

$$H(I, \phi) = \mathscr{H}(J, \theta). \tag{4.2}$$

The waves associated with the new variables will be called 'pseudo-waves'; those associated with (2.10) will be called 'physical waves'. The transformed action amplitudes are

$$\beta_k = I_k^{1/2} \mathrm{e}^{-\mathrm{i}\phi_k}. \tag{4.3}$$

The transformation (4.1) will be carried out as a continuous Lie transformation (Creamer *et al.* 1989). We choose a parameter λ,

$$0 \leqslant \lambda \leqslant 1,$$

and define canonical variables $\boldsymbol{Q}(\lambda)$, $\boldsymbol{P}(\lambda)$ such that

$$Q_k(0) = \theta_k, \quad P_k(0) = J_k, \quad Q_k(1) = \phi_k, \quad P_k(1) = I_k. \tag{4.4}$$

Equations to determine these variables are

$$\frac{\partial Q_k}{\partial \lambda} = \{Q_k, R\}, \quad \frac{\partial P_k}{\partial \lambda} = \{P_k, R\}, \tag{4.5}$$

where

$$R(\lambda) = R(\boldsymbol{P}(\lambda), \boldsymbol{Q}(\lambda))$$

is an appropriately chosen generating function. Related action amplitudes are

$$B_k(\lambda) = P_k^{1/2} \mathrm{e}^{-\mathrm{i}Q_k}, \tag{4.6}$$

satisfying the Poisson bracket relations

$$\{B_k(\lambda), B_{k'}(\lambda)\} = 0, \{B_k(\lambda), B_{k'}^*(\lambda)\} = -\mathrm{i}\delta_{k-k'}. \tag{4.7}$$

For integration of the transformation equations, we shall find that the form

$$\frac{\partial B_k}{\partial \lambda} = \{B_k, R\} \tag{4.8}$$

is more convenient than (4.5).

In the spirit of the expansion (2.15) we obtain from (4.5) and to the required order in ϵ

$$\left.\begin{aligned} \theta_k &= \phi_k - \epsilon \int_0^1 \mathrm{d}\lambda' \{Q_k, R\} = \phi_k - \epsilon \Delta\phi_k + O(\epsilon^2), \\ J_k &= I_k - \epsilon \int_0^1 \mathrm{d}\lambda' \{P_k, R\} = I_k - \epsilon \Delta I_k - \epsilon^2 \Delta^2 I_k + O(\epsilon^3). \end{aligned}\right\} \tag{4.9}$$

Here

$$\Delta\phi_k = \frac{\partial R(I, \theta)}{\partial I_k}, \quad \Delta I_k = -\frac{\partial R(I, \theta)}{\partial \theta_k}, \quad \Delta^2 I_k = -\frac{1}{2} \frac{\partial}{\partial \theta_k} \left[\sum_j \frac{\partial R(I, \theta)}{\partial \theta_j} \frac{\partial R(I, \theta)}{\partial I_j} \right]. \tag{4.10}$$

The prescription of the Kolmogorov 'super-convergent' perturbation theory (see Chirikov 1977) is to first make the transformation

$$\boldsymbol{J} \rightarrow \boldsymbol{I}, \quad \theta \rightarrow \theta$$

in the Hamiltonian. This leads to

$$H_x(I,\theta) = \mathscr{H}(I-\epsilon\Delta I-\epsilon^2\Delta^2 I,\theta) = \mathscr{H}_0(I)-\epsilon\sum_k \omega_k\,\Delta I_k+\epsilon\mathscr{H}_1(I,\theta)$$

$$-\epsilon^2\sum_k\frac{\partial\mathscr{H}_1}{\partial I_k}\Delta I_k+\epsilon^2\mathscr{H}_2(I,\theta)-\epsilon^2\sum_k\omega_k\,\Delta^2 I_k+O(\epsilon^3), \quad (4.11)$$

where we have used the relation

$$\frac{\partial\mathscr{H}_0}{\partial I_k}=\omega_k.$$

The next step is to split $\mathscr{H}_1$ into non-resonant and resonant parts,

$$\mathscr{H}_1 = \mathscr{H}_{1N}+H_{1R}. \quad (4.12)$$

The separation of $\mathscr{H}_1$ into non-resonant and resonant parts is somewhat arbitrary, except that $\mathscr{H}_{1N}$ must contain no terms for which f^+ or f^- (2.36) is very small. We shall here define (4.12) by the condition that H_{1R} contains only wave modes in D_R and each term in $\mathscr{H}_{1N}$ contains at least one wave mode that is in $D_{\bar{R}}$.

The non-resonant part is eliminated from (4.11) by proper choice of R:

$$\sum_k\omega_k\,\Delta I_k = \mathscr{H}_{1N}(I,\theta). \quad (4.13)$$

Using (4.13), we obtain then for (4.11)

$$\left.\begin{aligned} H_x(I,\theta) &= \mathscr{H}_0(I)+\epsilon H_{1R}(I,\theta)+\epsilon^2\mathscr{H}_{2T}+O(\epsilon^3),\\ \mathscr{H}_{2T}(I,\theta) &\equiv \mathscr{H}_2(I,\theta)-\sum_k\frac{\partial\mathscr{H}_1}{\partial I_k}\Delta I_k-\sum_k\omega_k\,\Delta^2 I_k. \end{aligned}\right\} \quad (4.14)$$

The next step in the Kolmogorov method is to average (4.11) over all angles θ. Such an average we represent by an overbar, so that for a function $L(I,\theta)$ we write

$$L(I,\theta) = \bar{L}(I)+\tilde{L}(I,\theta).$$

The averaged quantity (4.14) is then

$$H_0(I) = \bar{H}_x = \mathscr{H}_0+\epsilon^2\bar{\mathscr{H}}_{2T}, \quad (4.15)$$

where we have noted that

$$\bar{\mathscr{H}}_{1R}=0, \quad \overline{\Delta^2 I_k}=0.$$

The last step is to express θ in terms of ϕ in (4.11):

$$H(I,\phi) = H_1(I,\phi-\epsilon\Delta\phi) = H_0(I)+\epsilon H_{1R}(I,\phi)+\epsilon^2 H_2(I,\phi)+O(\epsilon^3). \quad (4.16)$$

Here

$$H_2(I,\phi)\equiv\tilde{\mathscr{H}}_{2T}-\sum_k\frac{\partial H_{1R}}{\partial\phi_k}\Delta\phi_k.$$

The required generating function R to give the relation (4.13), expressed in terms of the action amplitudes, is

$$R(\lambda) = -\sum_{k,l,m}[1/(32\mathscr{A}_0 V_k V_l V_m)]^{1/2}\left\{\delta_{k-l-m}\frac{\Gamma(\boldsymbol{k},\boldsymbol{l},\boldsymbol{m})}{(\omega_k-\omega_l-\omega_m)}[B_k^* B_l B_m+B_k B_l^* B_m^*]\right.$$

$$\left.+\tfrac{1}{3}\delta_{k+l+m}\frac{h(\boldsymbol{k},\boldsymbol{l},\boldsymbol{m})}{\omega_k+\omega_l+\omega_m}[B_k B_l B_m+B_k^* B_l^* B_m^*]\right\}, \quad (4.17)$$

where Γ and h are defined by (2.17). The reason that we do not tolerate terms containing a triad resonance is evident from the structure of (4.17). To be specific, at least one of the wave numbers $\boldsymbol{k}$, $\boldsymbol{l}$, $\boldsymbol{m}$ in (4.17) must lie outside the resonant domain D_R; that is, in the domain $D_{\bar{R}}$. Using (4.17), the transformation (4.8) is seen to be of the form

$$\frac{\partial B_k}{\partial \lambda} = \frac{\mathrm{i}}{4}\sum_{l,m}[1/(2\mathscr{A}_0 V_k V_l V_m)]^{1/2}\left\{\delta_{k-l-m}\frac{\Gamma(\boldsymbol{k},\boldsymbol{l},\boldsymbol{m})}{\omega_k-\omega_l-\omega_m}B_l B_m - 2\delta_{k+l-m}\frac{\Gamma(\boldsymbol{m},\boldsymbol{k},\boldsymbol{l})}{\omega_k+\omega_l-\omega_m}\right.$$
$$\left.\times B_m B_l^* + \delta_{k+l+m}\frac{h(\boldsymbol{k},\boldsymbol{l},\boldsymbol{m})}{\omega_k+\omega_l+\omega_m}B_l^* B_m^*\right\}. \quad (4.18)$$

We have now completed the first step in the Kolmogorov 'super convergent' perturbation theory. The next step would be to perform a second canonical transformation to remove the terms from H_2 not involving quartic resonances. (A clear description of this method has been given by Chirikov 1977.) Carrying out further steps in the perturbation theory is beyond our present scope. We shall instead split H_2 into two parts:

$$H_2 = H_{2R} + H_{2\bar{R}}. \quad (4.19)$$

The term H_{2R} contains only wave modes in D_R and each term in $H_{2\bar{R}}$ contains at least one wave mode that is in $D_{\bar{R}}$. We shall drop H_{2R} from (4.16) and adopt

$$H(\boldsymbol{I},\phi) = H_0(\boldsymbol{I}) + \epsilon H_{1R}(\boldsymbol{I},\phi) + \epsilon^2 H_{2R}(\boldsymbol{I},\phi) \quad (4.20)$$

as our Hamiltonian. We note that the only contribution to H_{2R} comes from $\mathscr{H}_2$, since the additional terms in H_2 must contain at least one wave mode not in D_R. With the simplification resulting from (4.20) we have lost the four-wave interactions for the longer wavelengths outside D_R. Because our primary interest is with three-wave interactions for capillary wave phenomena within D_R having very short interaction times, this approximation for the pseudo-wave amplitudes seems acceptable. For those longer wavelengths outside D_R the approximation (4.20) is identical with that used by Creamer *et al.* (1989).

4.1. *The pseudo-wave angular frequency*

From (4.15) we obtain the angular frequency of the free pseudo-waves as

$$\dot{\phi}_k \equiv \Omega_k = \frac{\partial K_0}{\partial I_k} \equiv \omega_k + \epsilon^2 \Delta\Omega_k + \ldots. \quad (4.21)$$

Introducing this represents an important step in the Kolmogorov method, since errors in the arguments of time-dependent phases of the waves will tend to destroy phase relations among Fourier components of wave structures.

The frequency (4.21) depends upon dynamical action variables and thus is in general time dependent. It turns out, however, that the time dependence is very weak for our applications. The reason for this is that for a wind wave spectrum the predominant contribution comes from those modes which are in $D_{\bar{R}}$ – in fact, from the smallest wavenumbers. When a wavenumber $l \in D_R$ it follows from (4.20) that the corresponding action variable I_l is a constant.

To evaluate $\Delta\Omega_k$ (which is linear in the I_l) we chose a Donelan–Pierson–Jähne model (similar to that given by Apel 1994) to provide the spectrum $\Psi(\boldsymbol{I})$ and thus the action variables I_l. The evaluated frequency was fitted numerically for $63 < k < 1000$ m^{-1} to a Fourier series in the angle θ_k between $\boldsymbol{k}$ and the wind velocity vector $\boldsymbol{U}_{10}$:

$$\Omega_k = \omega_k + kV_{st}\cos(\theta_k) + c_0 + c_1\cos(\theta_k) + c_2\cos(2\theta_k) + c_3\cos(3\theta_k) + \ldots. \quad (4.22)$$

Here

$$\left.\begin{aligned} V_{st} &= 0.028\,(U_{10}/10)\ln(97U_{10})\ \text{m s}^{-1} \\ c_0 &= 0.11+0.25\,(U_{10}/10)\ \text{s}^{-1}, \\ c_1 &= -0.10+0.50\,(U_{10}/10)^{1/2}\ \text{s}^{-1}, \quad c_2, c_3, \ldots \approx 0.01\ \text{s}^{-1}. \end{aligned}\right\} \tag{4.23}$$

The quantity V_{st} corresponds to the Stokes drift and can make a significant contribution to Ω_k (compare the discussion of this in Watson & McBride 1993). The k-dependence of c_0 and c_1 is weak and was not taken into account in (4.23).

To estimate the dynamic fluctuation in time arising from those I_l within D_R, we have used the output of a numerical evaluation of the action amplitudes (from integration of (2.31)) to calculate (4.21). This gave a time-fluctuating contribution of about 0.01 s^{-1} to Ω_k, which seems negligible for our applications.

Because of the small values of the coefficients in (4.23) we can therefore take as an adequate approximation for the pseudo-wave angular frequency

$$\Omega_k = \omega_k + \boldsymbol{k}\cdot\hat{U}V_{st}. \tag{4.24}$$

4.2. *Equations of motion*

The equations of motion for the pseudo-wave action amplitudes (4.3) are

$$\dot{\beta}_k = \{\beta_k, H\}. \tag{4.25}$$

Using (2.12) and (4.20), we obtain

$$\dot{\beta}_k + \mathrm{i}\Omega_k\beta_k = 0, \quad \boldsymbol{k}\in D_{\bar{R}}, \tag{4.26}$$

since the interactions in (4.20) involve only wave modes in D_R. For wave modes in D_R we obtain the equations

$$\begin{aligned} \dot{\beta}_k + \mathrm{i}\Omega_k\beta_k = \sum_{l,p}[1/(32\mathscr{A}_0 V_k V_l V_m)]^{1/2}\{&\delta_{k-l-p}\Gamma(\boldsymbol{k},\boldsymbol{p},\boldsymbol{l})\beta_l\beta_p \\ &-2\delta_{k-l+p}\Gamma(\boldsymbol{l},\boldsymbol{k},\boldsymbol{p})\beta_l\beta_p^* + \delta_{k+l+p}h(\boldsymbol{l},\boldsymbol{p},\boldsymbol{k})\beta_l^*\beta_p^*\} \\ &+\text{four-wave terms,}\quad \text{all waves}\in D_R. \end{aligned} \tag{4.27}$$

For our present application to one surface dimension the discrete modes k, l, ... are specified by the first of equations (2.8).

To reduce the number of modes in (4.27), we introduce again the grid (2.27), (2.28), and (2.29). The modes in both D_R and D_S form the set

$$D_{RS} = D_R \cap D_S. \tag{4.28}$$

Those modes in D_R, but not in D_S, form the set

$$D_{R\bar{S}} = D_R \cap D_{\bar{S}}. \tag{4.29}$$

A special class of initial conditions at $t = 0$ is assumed for (4.27):

$$\beta_k(0) = 0, \quad \boldsymbol{k}\in D_{R\bar{S}}; \quad \beta_k(0) = \beta_{k0}, \quad \boldsymbol{k}\in D_{RS}, \tag{4.30}$$

where β_{k0} is an assigned initial value. Because of the specific form of (2.27), integration of (4.27) will lead to (as was the case for (2.30))

$$\beta_k(t) = 0, \quad \text{all } t, \quad \boldsymbol{k}\in D_{R\bar{S}}. \tag{4.31}$$

We may thus ignore all amplitudes in $D_{R\bar{S}}$ when integrating the equation set (4.27). This can clearly substantially reduce the computational burden for these equations.

We emphasize that (4.30) represent initial conditions on the pseudo-wave, not on the physical wave, amplitudes. We are led to these initial conditions, noting that: (i) we

must be somewhat empirical in assigning initial conditions to the pseudo-waves; (ii) for large systems with many degrees of freedom bulk properties tend to be largely independent of specific dynamic orbits (for example, the thermodynamic properties of a gas in a bottle seem very insensitive to the specifics of the molecular orbits); (iii) we can vary the fetch and the grid, which effectively changes the conditions (4.30).

At this point it may be helpful to summarize our classification of wavenumber sets:

$$\left.\begin{aligned}
&D \text{ is the full set (2.8) in } \mathscr{A}_0,\\
&D_R \text{ is the triad resonance set,}\\
&D_{\bar{R}} \text{ is the set not in } D_R,\ D_R \cup D_{\bar{R}} = D,\\
&D_S \text{ is the set (2.28),}\\
&D_{\bar{S}} \text{ is the set not in (2.28),}\\
&D_{RS} = D_R \cap D_S \text{ is the subset of } D_S \text{ that is in } D_R,\\
&D_{R\bar{S}} \text{ is the set that is in } D_R \text{ but not in } D_S,\\
&D_{\bar{R}S} \text{ is the set that is in } D_S \text{ but not in } D_R.
\end{aligned}\right\} \tag{4.32}$$

For numerical evaluation of (4.27) it is convenient to replace the action amplitudes by wave slope amplitudes α_k, as in (2.19):

$$\beta_k = -\mathrm{i}(\mathscr{A}_0 V_k/2)^{1/2}\,\alpha_k\,\mathrm{e}^{-\mathrm{i}\Omega_k t}/k. \tag{4.33}$$

The vertical pseudo-displacement of the water surface, expressed in terms of these slope amplitudes, is

$$\hat{\zeta}(\boldsymbol{x}, t) = \sum_{\boldsymbol{k}} 1/(2k)\,[\alpha_{\boldsymbol{k}}\,\mathrm{e}^{\mathrm{i}(\boldsymbol{k}\cdot\boldsymbol{x}-\Omega_k t)} + \text{c.c.}]. \tag{4.34}$$

Since we can ignore wave modes not in D_{RS}, the reduced set of equations (4.27) expressed in terms of the α_k have a structure identical to (2.31):

$$\dot{\alpha}_{\boldsymbol{K}} + \epsilon_1\,[\mathrm{i}\beta\alpha_{\boldsymbol{K}}] = \epsilon_3\,T_3(\alpha; \boldsymbol{K}) + \epsilon_4\,T_4(\alpha; \boldsymbol{K}). \tag{4.35}$$

Because of special form of the nonlinear frequency shift (4.24), we have

$$\Omega_K - \Omega_L - \Omega_P = \omega_K - \omega_L - \omega_P,$$

etc. in T_3 and T_4, leaving these unchanged. Thus, the only difference from (2.31) is that now the modes $\boldsymbol{K}$, $\boldsymbol{L}$, $\boldsymbol{P}$, ..., are restricted to the set D_{RS}, rather than the set D_S. Since the number of modes in D_{RS} may be substantially less than the number in D, a major reduction in computing time can be achieved.

After integrating the equation set (4.35), we must obtain the physical wave amplitudes by integrating (4.18). To do this in the present paper we shall restrict ourselves to waves in one surface dimension and, as in §3, we also continue to restrict the waves in set D (2.8) to positive wavenumbers, $k_x, \ldots > 0$.

In analogy to (4.33), we introduce generalized slope amplitudes with the relation

$$B_k(\lambda) = -\mathrm{i}(\mathscr{A}_0 V_k/2)^{1/2}\,A_k(\lambda)\,\mathrm{e}^{-\mathrm{i}\Omega_k t}/k, \tag{4.36}$$

where

$$A_k(1) = \alpha_k, \quad A_k(0) = a_k\,\mathrm{e}^{\mathrm{i}(\Omega_k - \omega_k)t} \equiv \tilde{a}_k. \tag{4.37}$$

Here a_k is defined by (2.19). We expect the frequency shift $(\omega_k - \Omega_k)$ to be significant only when there is a strong Stokes drift. The transformation (4.18) may now be written in the form

$$\frac{\partial A_k}{\partial \lambda} = \sum_m M_{km}\,A_m. \tag{4.38}$$

With $l = k-m, k, m > 0$, we obtain from (4.18)

$$M_{km} = \begin{cases} \dfrac{k^2(\omega_m/\omega_k)\,\omega_l A_l}{2|l|m(\omega_k-\omega_m-\omega_l)} e^{i(\Omega_k-\Omega_l-\Omega_m)t}, & l>0, l<m, \\ \dfrac{k^2(\omega_m/\omega_k)\,\omega_l A_l}{4|l|m(\omega_k-\omega_m-\omega_l)} e^{i(\Omega_k-\Omega_l-\Omega_m)t}, & l>0, l=m, \\ \dfrac{k^2\omega_l A_{-l}^*}{2|l|m(\omega_k-\omega_m+\omega_l)} e^{i(\Omega_k+\Omega_l-\Omega_m)t}, & l<0, |l|<m, \\ 0 \quad \text{otherwise.} \end{cases} \tag{4.39}$$

The wavenumbers k, m, $|l|$ above are in set D (2.8). The sum in (4.38) is restricted to give allowed values of l, which include the condition that

$$A_l = 0, \quad l < 0.$$

Since at least one of the three wavenumbers k, m, $|l|$ must lie in $D_{\bar{R}}$, we have the following possibilities:

$$k \in D_R, \quad \text{then } |l| \in D_R \quad \text{and} \quad m \in D; \quad k \in D_{\bar{R}}, \quad \text{then } |l|, m \in D. \tag{4.40}$$

Equations (4.38) are to be integrated from $\lambda = 1$ to 0. The initial conditions on the $A_k(\lambda)$ are (see (4.26) and (4.30))

$$\left.\begin{aligned} &A_k(1) = 0, \quad k \in D_{R\bar{S}}, \\ &A_k(1) \text{ is obtained from integration of (4.35) for } k \in D_{RS}, \\ &A_k(1) \text{ is assigned as an initial condition for } k \in D_{\bar{R}}. \end{aligned}\right\} \tag{4.41}$$

As an illustration of our use of mode sets, let us consider grid G_1 of table 1 with $\lambda_c = \frac{2}{3}$ cm, $S_x = 10$ cm. The fetch X of $\mathscr{A}_0$ is taken as 60 cm. Then, there are 90 modes in D. The number of modes appearing in (4.35), i.e. in D_{RS}, is 15. There are 5 modes in $D_{\bar{R}}$ and 70 in $D_{R\bar{S}}$. We thus need evaluate (4.35) for only 15 pseudo-wave modes and will have 90 physical wave mode amplitudes output from (4.38).

In practice, the coupled equations in (4.38) are relatively simple and fast to integrate when the number of modes does not exceed a few hundred. (For the example just described having 90 complex amplitudes, (4.38) represent 180 coupled nonlinear equations. Integration time on a Macintosh computer was about 10 s.) A second-order Runge–Kutta scheme sufficed, but a Bulirsch–Stoer algorithm (Press *et al.* 1992) was faster and has been used for our calculations. We emphasize that (4.38) is not a dynamic equation in that time appears in it only as a parameter.

Numerical integration of (4.38) is not practical, however, for a wind wave spectrum extending to wavelengths of tens of metres. Fortunately, an analytic approximation for the effects of these longer waves is available. To develop this, we suppose the area $\mathscr{A}_0$ to be imbedded in a much larger area $\mathscr{A}_L$. The dimensions of $\mathscr{A}_0$ are chosen to give a practical set of modes for integration of (4.38) and $\mathscr{A}_L$ is assumed to include all waves in the wind wave spectrum.

From the solution of (4.38), producing the mode amplitudes in $\mathscr{A}_0$, we can construct the complex surface displacement

$$Z(x) = \sum_k \tilde{a}_k e^{i(kx-\Omega_k t)}/(2ik), \tag{4.42}$$

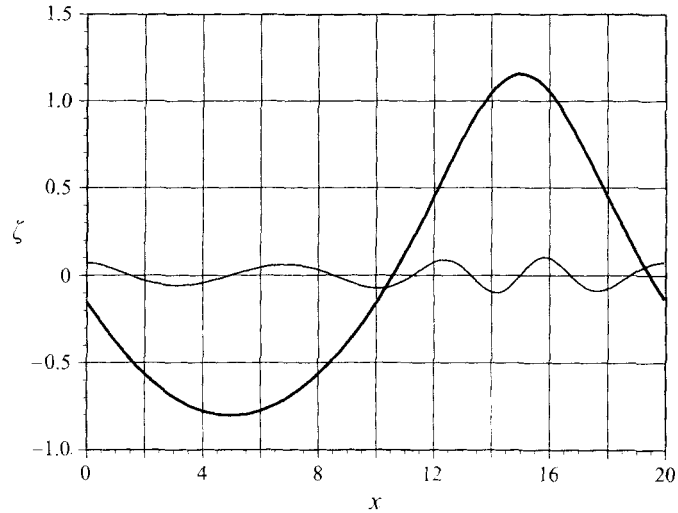

FIGURE 7. Illustration of Lie transform pairs. Heavy curve is transform of 20 cm wavelength wave of slope 0.3. Light curve is transform of 5 cm wave of slope 0.1 interacting with the longer wave.

where $\zeta = -2\,\mathrm{Im}(Z)$, see (2.5). It is shown in Appendix B (equation (B 10)) that the effect of the longest waves is given by replacing (4.42) by

$$Z(x) = \sum_k \tilde{a}_k \mathrm{e}^{\mathrm{i}(kx - \mathscr{D}(x) - \Omega_k t)}/(2\mathrm{i}k), \tag{4.43}$$

where $\mathscr{D}(x)$ is the horizontal fluid displacement due to orbital currents of the larger waves and (4.43) describes effects of advection and straining. We may assume linear waves for the evaluation of $\mathscr{D}(x)$.

5. Applications of the Lie transform

In this section we continue the discussion begun in §3 of radiated capillary waves and of wind waves using the Lie transform technique to increase the wave fetch.

5.1. *Lie transform pairs*

The transform (4.38) associates with any pseudo-wave a corresponding physical wave, irrespective of the use of (4.35). We illustrate this with two simple examples.

For these we use the grid G_1 of table 1 and set the fetch of $\mathscr{A}_0$ to $X = 20$ cm. For the first example, the pseudo-wave is a sine wave of wavelength 20 cm and slope 0.3. This wave is a member of the set D_R. All other pseudo-waves have zero amplitude. In figure 7 the surface displacement ζ_1 of the physical wave is shown by the heavy line. The sharpening of crests and flattening of troughs is a characteristic of the Lie transform (compare Creamer *et al.* 1989).

For the second example, the pseudo-wave field is represented by the sum of two sine waves. The first is that used above, having a wavelength of 20 cm and a slope of 0.3. The second is a sine wave of 5 cm wavelength and slope of 0.1. The displacement of the resulting physical wave is written as

$$\zeta_2 = \zeta_1 + \delta\zeta,$$

where $\delta\zeta$ represents the incremental effect of the shorter wave. The light curve in figure 7 shows the quantity $\delta\zeta$. The 5 cm wave, riding on the larger wave, is both modulated and subject to straining.

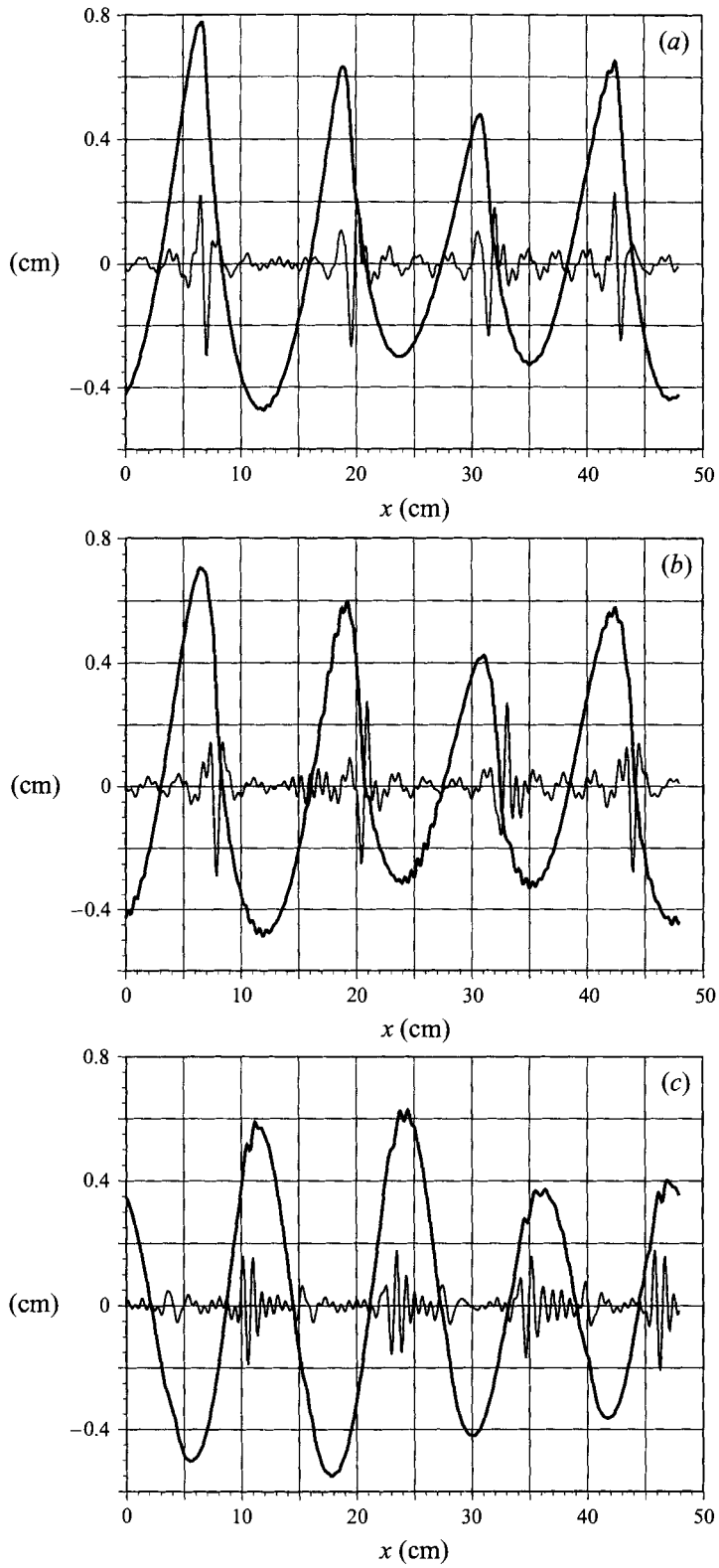

FIGURE 8(*a–c*). For caption see facing page.

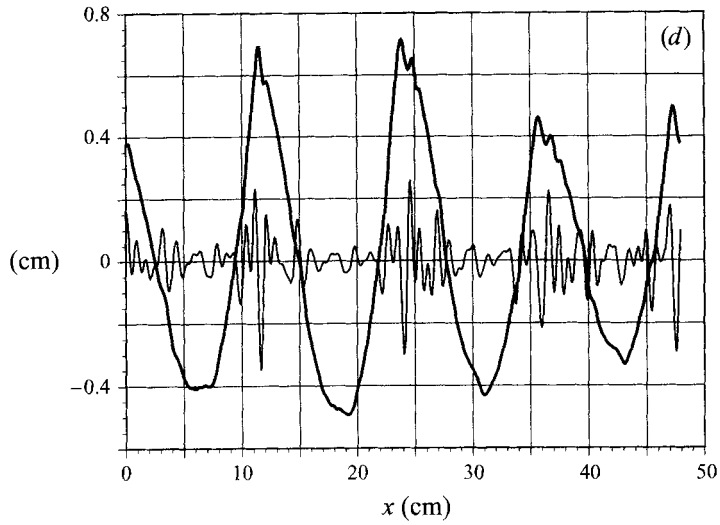

FIGURE 8. The wave resulting from a pseudo-wave consisting of a 12 cm wavelength sine wave of slope 0.25 and a 16 cm sine wave of slope 0.05. Dissipation was assumed; (*a*, *c*) were calculated for three-wave interactions only, (*b*, *d*) were calculated with both three- and four-wave interactions. Heavy curve is surface displacement and light curve is F_m filtered slope. Time is 0.2 s in (*a*, *b*) and 0.6 s in (*c*, *d*).

5.2. *Modulated sine wave*

We now consider a pseudo-wave system consisting at time $t = 0$ of a 12 cm wave-length sine wave of slope 0.25 and a 16 cm sine wave of slope 0.05. The area $\mathscr{A}_0$ has a fetch $X = 48$ cm. The grid G_3 of table 1 is used, so the shorter wave is in D_R and the longer wave is in $D_{\bar{R}}$. Equations (4.35) were integrated with dissipation. For figure 8(*a*, *c*) integration was done with only the three-wave interactions ($\epsilon_1 = \epsilon_3 = 1$, $\epsilon_4 = 0$). For figure 8(*b*, *d*) both three- and four-wave interactions were used ($\epsilon_1 = \epsilon_3 = \epsilon_4 = 1$). In figure 8 the heavy curves represent surface displacement and the light curves F_m filtered slope.

The time for figure 8(*a*, *b*) is $t = 0.2$ s. The surface roughness tends to be ahead of the longer wave crests; this is more pronounced in figure 8(*b*) with the use of the four-wave term T_4. The four-wave term also leads to slightly enhanced roughness, a result we observed in §3.

For figure 8(*c*, *d*) the time is 0.6 s. The surface roughness is now more centred under the long wave crests, otherwise figure 8(*c*) appears much like figure 8(*a*). We see in figure 8(*d*) that the four-wave interaction has led to greater roughness in the wave troughs.

Continuing the calculation to later times shows a gradual increase in the contribution from the four-wave interactions. Comparison of surface displacement shows crest sharpening that is quite similar for the three-wave and three- and four-wave cases, however.

Figure 8(*a*) is similar to figure 2(*b*), except that in figure 8(*a*) the fine-scale slope amplitude is greater and is modulated by the crest height of the longer wave. The Lie transform tends to enhance longer wave crests. Because of the small slope (i.e. 0.05) of the longer wave in figure 8, modulation effects are relatively weak. This is in contrast to the case shown in figure 2(*c*), for which the modulating wave is very steep.

We again consider the wave system that was studied in figure 8, except that we now vary the amplitude of the 12 cm wave. The slope of the 16 cm wave remains constant

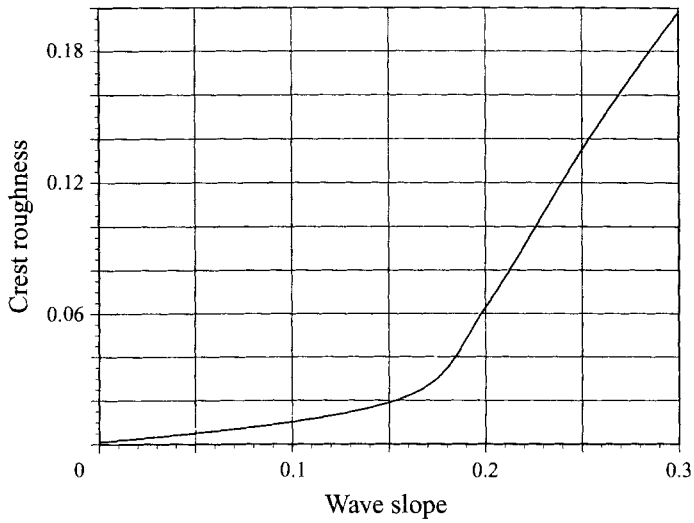

FIGURE 9. Illustration of r.m.s. F_m filtered slope near crests, i.e. crest roughness, as a function of the slope of a 12 cm wavelength sine wave interacting with a 16 cm sine wave of fixed slope = 0.05.

at 0.05. We calculate, with dissipation and using three- and four-wave interactions ($\epsilon_1 = \epsilon_3 = \epsilon_4 = 1$), the fine-scale roughness as the r.m.s. F_m filtered slope averaged over spatial intervals for which the surface displacement is positive. We show this as crest roughness *vs.* 12 cm wave lope in figure 9.

5.3. *Wind waves*

We now consider wave amplitudes initiated by the Donelan–Pierson (1987) spectrum and given random phases, as described in §3. We again interpret these initial conditions as applying to pseudo-waves. We first produce in this manner a set of initial values for those α_K for which K is in D_{RS}. With these we integrate (4.35) to produce at time t the amplitudes

$$A_k(1) = \alpha_k(t), \quad k \in D_{RS} \tag{5.1}$$

(see (4.41)). For those $k \in D_{\bar{R}}$ we again use the Donelan–Pierson spectrum and the random phase generator to give $A_k(1)$. For the remaining amplitudes we have, according to (4.41),

$$A_k(1) = 0, \quad k \in D_{R\bar{S}}.$$

We shall calculate the capillary spectrum for a wind speed of 4 m s^{-1}, choosing the grid G_3 of table 1 and the fetch of the area $\mathscr{A}_0$ as $X = 48$ cm. The spectrum for $U_{10} =$ 4 m s^{-1} extends to wavelengths $\lambda \approx 10$ m. To account for these longest waves, we consider (as described in §4) the area $\mathscr{A}_0$ to be imbedded in a much larger area $\mathscr{A}_L$. We suppose the fetch of $\mathscr{A}_L$ to be

$$X_L = J_L X, \tag{5.2}$$

where J_L is an integer (compare (2.27)) and $X_L \gg 10$ m is large enough to include the entire wind wave spectrum. The relation (5.2) lets us assume that the wave modes in $\mathscr{A}_0$ are also modes of the set D_L in $\mathscr{A}_0$ (although sparse in the larger area). The wave amplitudes that are in D_L and have wavelengths less than X, but are not in D, are set equal to zero at time $t = 0$ and because J_L is an integer these remains zero until the long-wave part of the inverse Lie transformation is performed (Appendix B).

The Donelan–Pierson spectrum and a random number generator are used to provide initial pseudo-wave amplitudes. Integration of (4.35) and (4.38) provides the physical wave amplitudes in D. From these we can calculate the complex displacement $Z(x)$, see (4.42).

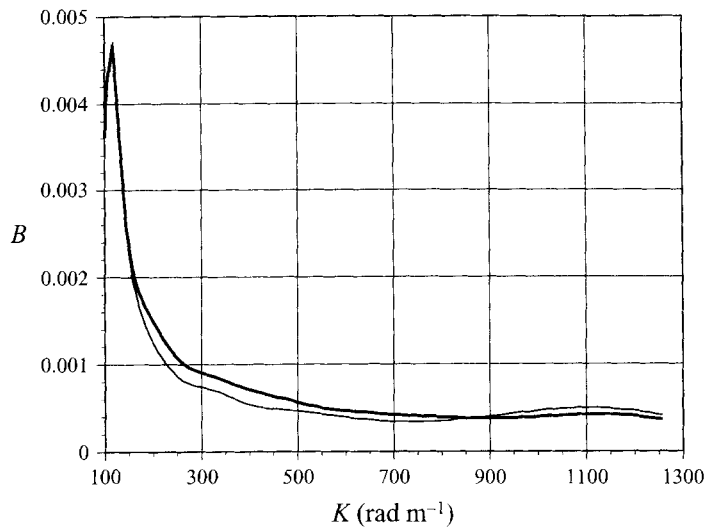

FIGURE 10. Wave spectrum B at $t = 0.3$ s for a wind speed of 4 m s^{-1}. Calculation was done with dissipation. The light curve shows the spectrum using only the three-wave interactions. The heavy curve shows the spectrum using both the three- and four-wave interactions.

The horizontal displacement $\mathscr{D}(x)$ (see (B 6)) may be expressed as

$$\mathscr{D}(x) = -\sum_l [a_l \mathrm{e}^{\mathrm{i}(lx-\omega_l t)} - \text{c.c.}]/(2\mathrm{i}l), \tag{5.3}$$

where the sum is over wave modes in D_L, but with wavelengths significantly larger than X. We assume that the a_l represent Gaussian variables with mean-square magnitudes given by the Donelan–Pierson spectrum. With the quantity (5.3) we can evaluate (4.43).

The Fourier transform of $Z(x)$, (4.43), in D_L is

$$\tilde{Z}_k = \frac{1}{X_L}\int \mathrm{d}x\, \mathrm{e}^{-\mathrm{i}kx} Z(x), \tag{5.4}$$

where k is a wavenumber in D_L. The displacement spectrum $\Psi(k,0)$ in the downwind direction is given by

$$\Delta_L^2 K\Psi(k,0) = \langle |\tilde{Z}_k|^2 \rangle_{LW}, \tag{5.5}$$

where $\langle \ldots \rangle_{LW}$ implies an ensemble average over the long-wave modes in $\mathscr{D}_L$ and $\Delta_L^2 K$ represents a wavenumber interval in D_L. On following the similar argument of Watson & McBride (1993), we obtain

$$\Delta_L^2 K\Psi(k,0) = \sum_p \frac{1}{X_L}\int \mathrm{d}r\, \mathrm{e}^{\mathrm{i}(p-k)r} \exp\{-p^2[C(0)-C(r)]\}\frac{|\tilde{a}_p|^2}{2p^2}. \tag{5.6}$$

Here the $\tilde{a}_p$ are defined by (4.37), the p are wavenumbers in the set D, the k are members of the set D_L, and

$$C(x-y) = C(y-x) = \langle \mathscr{D}(x)\mathscr{D}(y) \rangle_{LW}. \tag{5.7}$$

As a final step we average the quantity (5.6) over five realizations of the $\tilde{a}_p$.

In figure 10 we show as the light curve the dimensionless spectrum $B = K^4\Psi$, as calculated from (5.6). The initial amplitude data of figure 5(*a*) were used. The time is $t = 0.3$ s, dissipation was assumed and the four-wave term was not used ($\epsilon_1 = \epsilon_3 = 1$, $\epsilon_4 = 0$). The calculation was repeated with the same input data set, but with both the

three- and four-wave interactions ($\epsilon_1 = \epsilon_3 = \epsilon_4 = 1$). The resulting spectrum at $t = 0.3$ s is shown as the heavy curve in figure 10. Comparison of the two curves shows only modest effects of the four-wave interactions. We note that the dense set of k-values and the smoothing effect in (5.6) permits plotting the spectra in figure 10 as continuous curves.

In Part 2 of this work the discussion of wind waves and of surface roughness will be extended to two surface dimensions.

6. Conclusions

In §3 we calculated properties of three kinds of wave systems, beginning with the rather simple Wilton triad. Perhaps the most significant observation from these calculations is the role of triad resonances, as evidenced by the dependence on f_{lim}, (2.40). The values required for f_{lim} were too large to justify a simple triad resonance model, such as that of the Hasselmann theory. Important channels for energy flow occur away from triad resonance regions, as was evidenced from the simple example of the Wilton harmonic triad and from the calculation of wind wave spectra. On the other hand, values of f_{lim} as large as the maximum possible resonance mismatch were not required. The minimum required values of f_{lim} for the four-wave terms were roughly one-half the values required for the three-wave terms. Significant effects resulting from off-resonant triad interactions have also been found by Freilich & Guza (1984) in their study of gravity waves in shallow water.

We saw that off-resonance interactions were found to lead to significant corrections to the Hasselmann method. Energy transfer to the capillary spectrum occurred over a broader spectral domain than that resulting from triad resonance mechanisms alone. The total energy transfer rates, as shown in table 2, were in order of magnitude agreement, however.

We saw that ripples of a few millimetres wavelength tend to be on the forward face of steep waves, but that those in the centimetre range tend to be more nearly coincident with the wave crests. Modulation of these waves by waves of larger wavelength can change this ripple structure. The variation of crest roughness with wave slope was illustrated in figure 9.

Calculations were compared using only the three-wave interactions and using the three- and four-wave interactions. For the fast time scales of capillary wave phenomena the three-wave terms only gave results that were generally qualitatively, or semi-quantitatively, consistent with those calculated using three- and four-wave interactions. Additional fine-scale waves generated by the four-wave interactions were seen to cause an interference pattern for the three-wave-generated fine-scale waves.

We have adopted for this work a rather inefficient specification for the resonant domain D_R. This was done in the interest of simplicity and also because for our applications to one-dimensional waves a more efficient calculation was not needed. The great majority of the three-wave interaction terms in (2.31) are far from resonance and could have been transformed out of (2.31) by the canonical transformation. Keeping these terms adds to the computational burden in two ways: first, we have had to numerically evaluate unnecessary interaction terms; second, these terms, being far from a triad resonance have rapidly oscillating exponentials that slow numerical integration. (When the Kolmogorov technique is extended one more order to the four-wave terms, similar considerations apply.) When we investigate in Part 2 wave phenomena in two surface dimensions, we shall have need for a more efficient choice of resonance domains and will then address this issue.

We would like to thank M. Longuet-Higgins and W. K. Melville for helpful discussions relating to this work and, in particular, to the radiation of millimetre-wavelength capillary waves.

One of us (K.M.W.) received partial support for this work from Office of Naval Research Grant N00014-94-10013.

Appendix A. Interaction with the external environment

We imagine the wave system to be in interaction with a large-scale 'heat bath' that can give to it, or extract from it, energy. The total Hamiltonian will be of the form

$$\mathscr{H}_T = \mathscr{H}(\boldsymbol{J}, \theta) + \mathscr{H}_E(\boldsymbol{J}, \theta, \boldsymbol{Z}), \tag{A 1}$$

where $\mathscr{H}$ is given by (2.15), $\mathscr{H}_E$ represents the coupling of the external environment, and $\boldsymbol{Z}$ represents external degrees of freedom. The canonical transformation is carried out as in §4:

$$\boldsymbol{J} \to \boldsymbol{P}(\lambda) \to \boldsymbol{I}, \quad \theta \to \boldsymbol{Q}(\lambda) \to \phi, \quad \boldsymbol{Z} \to \boldsymbol{Z} \to \boldsymbol{Z}. \tag{A 2}$$

The resulting Hamiltonian is

$$H_T = H(\boldsymbol{I}, \phi) + H_E(\boldsymbol{I}, \phi, \boldsymbol{Z}). \tag{A 3}$$

Equations (4.25) for the pseudo-wave amplitudes are now of the form

$$\dot{\beta}_{\boldsymbol{k}} = \{\beta_{\boldsymbol{k}}, H\} + \{\beta_{\boldsymbol{k}}, H_E\}. \tag{A 4}$$

We use the second term as a phenomenological source for energy input from the wind (with a Miles 1957 model, for example) and/or sink for energy loss due to viscous dissipation.

Appendix B. Simplification of Lie transform for long waves

As was described in §4, the Lie transformation equations are impractical to integrate numerically for a very broad spectrum. A useful analytic approximation that removes this restriction can be developed for (4.18) for this case.

First, we recall from the work of Creamer *et al.* (1989) and Watson & McBride (1993) that the Lie transformation has a relatively weak effect on the longer gravity waves. Thus, we assume that

$$B_l(1) \approx B_l(0) \tag{B 1}$$

for these longer waves. We may therefore analyse (4.18) for only those $\boldsymbol{k}$ that are in the capillary and short gravity wave range. This suggests that we can rewrite (4.18) in the form

$$\frac{\partial B_{\boldsymbol{k}}}{\partial \lambda} = g_1(\boldsymbol{k}) + g_0(\boldsymbol{k}), \tag{B 2}$$

where $g_0(\boldsymbol{k})$ contains those terms on the right in (4.18) that have a wavenumber (label this as $\boldsymbol{l}$) much less in magnitude than k.

Creamer *et al.* (1989) and Watson & McBride (1993) showed that the form of g_0 can be written as

$$g_0(\boldsymbol{k}) \approx -\frac{\mathrm{i}}{(2A_0)^{1/2}} \sum_{l(l \ll k)} (V_k/V_l)^{1/2}\, \hat{\boldsymbol{l}} \cdot [(\boldsymbol{k}-\boldsymbol{l})\, B_{k-l} B_l / V_{|k-l|}^{1/2} + (\boldsymbol{k} \times \boldsymbol{l})\, B_{k+l} B_l^* / V_{|k+l|}^{1/2}]. \tag{B 3}$$

The remaining terms in (4.18) are included in g_1. Now Watson & McBride (1993) observed that

$$\bar{g}_0(\boldsymbol{x}) \equiv \sum_k e^{i\boldsymbol{k}\cdot\boldsymbol{x}} g_0(\boldsymbol{k})/(2\mathscr{A}_0 V_k)^{1/2} \approx \mathscr{D}(\boldsymbol{x})\cdot\nabla Z(\boldsymbol{x}), \tag{B 4}$$

where

$$Z(\boldsymbol{x}) = \sum_k e^{i\boldsymbol{k}\cdot\boldsymbol{x}} B_k/(2\mathscr{A}_0 V_k)^{1/2} \tag{B 5}$$

and

$$\mathscr{D} = -\sum_l \hat{\boldsymbol{l}}[B_l e^{i\boldsymbol{l}\cdot\boldsymbol{x}} + \text{c.c.}]/(2\mathscr{A}_0 V_l)^{1/2}. \tag{B 6}$$

We note from (2.5) that the vertical displacement of the surface is

$$\zeta(x) = -2\,\mathrm{Im}\,(Z(x)), \quad \lambda = 0,$$

and also note that at $\lambda = 0$ $\mathscr{D}$ corresponds (in the linear wave approximation) to the horizontal fluid displacement due to the orbital current.

If we were to neglect the term g_0 in (B 2), we would have an equation of the form

$$\frac{\partial B_k^0}{\partial \lambda} = g_1^0(\boldsymbol{k}), \tag{B 7}$$

where g_1^0 is g_1 with B_k replaced by B_k^0, which represents the solution of (B 7). We note that (B 7) is unchanged by a phase shift of the form

$$B_k^0 \to e^{i\boldsymbol{k}\cdot\boldsymbol{d}} B_k^0,$$

corresponding to a displacement $\boldsymbol{d}$ in x-space.

Now, following the work of Creamer *et al.* (1989), Watson & McBride (1993) showed that the expression

$$Y(\boldsymbol{u}) = \sum_k e^{i\boldsymbol{k}\cdot\boldsymbol{u}} c_k \tag{B 8}$$

is a solution of the equation

$$\frac{\partial Y}{\partial \lambda} = \mathscr{D}\cdot\nabla Y$$

if

$$\boldsymbol{u} = \boldsymbol{x} + (\lambda - 1)\,\mathscr{D}(\boldsymbol{u}) \tag{B 9}$$

and c_k does not depend on λ. (The solution (B 9) depends on the scale separation $l \ll k$ and is valid up to first order in $|\nabla\mathscr{D}|$.) We see now that the required solution to (B 2) is, in x-space,

$$Z(\boldsymbol{x}) = \sum_k e^{i\boldsymbol{k}\cdot\boldsymbol{u}} B_k^0/(2\mathscr{A}_0 V_k)^{1/2}. \tag{B 10}$$

That is,

$$\frac{\partial Z}{\partial \lambda} = \sum_k \left\{ e^{i\boldsymbol{k}\cdot\boldsymbol{u}} \frac{\partial B_k^0}{\partial \lambda} + \sum_k B_k^0 \frac{\partial}{\partial \lambda}[e^{i\boldsymbol{k}\cdot\boldsymbol{u}}] \right\} \Big/ (2\mathscr{A}_0 V_k)^{1/2}. \tag{B 11}$$

The second term in (B 11) is of the form (B 8) and this is just the expression (B 4). We use (B 7) and the invariance under a phase shift to see that the first term in (B 11) is just the first term in (B 2). (We use again the condition of scale separation to argue that $\mathscr{D}$ is effectively constant over the short-wavelength waves.) The anticipated weak dependence of the long waves on the Lie transformation lets us use (B 1) to set

$$\mathscr{D}(\boldsymbol{u}) \approx \mathscr{D}(\boldsymbol{x}). \tag{B 12}$$

To integrate equations (4.18) for the inverse Lie transformation, we must first decide at what wavenumbers to make the scale separation implied in (B 2). We must next integrate (B 7), which we shall find to be much simpler than the full set (4.18). Finally, the effect of g_0 of (B 3) is accounted for in the analytic expression (B 10). When (B 7) is re-expressed in terms of the slope variables of (4.36), it becomes (4.38).

REFERENCES

APEL, J. R. 1994 An improved model of the ocean surface wave vector spectrum and its effects on radar backscatter. *J. Geophys. Res.* **99**, 16269–16291.

BENJAMIN, T. B. 1967 Instability of periodic wavetrains in nonlinear dispersive systems. *Proc. R. Soc. Lond.* A **299**, 59–75.

BENJAMIN, T. B. & FEIR, J. E. 1967 The disintegration of wave trains in deep water. Part 1. Theory. *J. Fluid Mech.* **27**, 417–430.

CHIRIKOV, B. V. 1977 A universal instability of many-dimensional oscillator systems. *Phys. Rep.* **52**, 264–379.

COHEN, B. L., WATSON, K. M. & WEST, B. J. 1976 Some properties of deep water solitons. *Phys. Fluids* **19**, 345–354.

COX, C. S. 1958 Measurements of slopes of high-frequency wind waves. *J. Mar. Res.* **16**, 199–225.

CREAMER, D., HENYEY, F., SCHULT, R. & WRIGHT, J. 1989 Improved linear representation of ocean surface waves. *J. Fluid Mech.* **205**, 135–161.

DONELAN, M. & PIERSON, W. 1987 Radar scattering and equilibrium ranges in wind-generated waves with applications to scatterometry. *J. Geophys. Res.* **92**, 4971–5030.

DUNCAN, J. H., PHILOMIN, V., BEHRES, M. & KIMMEL, J. 1994 The formation of spilling breaking water waves. *Phys. Fluids* **6**, 2558–2560.

EBUCHI, N., KAWAMURA, H. & TOBA, Y. 1987 Fine structure of laboratory wind wave surfaces studied using optical method. *Boundary-Layer Met.* **39**, 133–151.

FREILICH, M. H. & GUZA, R. T. 1984 Nonlinear effects on shoaling surface gravity waves. *Phil. Trans. R. Soc. Lond.* A **311**, 1–41.

GASTEL, K. VAN 1987*a* Nonlinear interactions of gravity-capillary waves: Lagrangian theory and effects on the spectrum. *J. Fluid Mech.* **182**, 499–523.

GASTEL, K. VAN 1987*b* Imaging by X-Band radar of subsurface features: A nonlinear phenomena. *J. Geophys. Res.* **92**, 11857–11866.

GOLDSTEIN, H. 1969 *Classical Mechanics*. Addison-Wesley.

HASSELMANN, K. 1968 Weak-interaction theory of ocean waves. In *Basic Developments in Fluid Mechanics* (ed. M. Holt), pp. 117–182. Academic.

HENDERSON, D. M. & HAMMACK, J. 1987 Experiments on ripple instabilities: Part 1. Resonant triads. *J. Fluid Mech.* **184**, 15–41.

HOLLIDAY, D. 1977 On nonlinear interactions in a spectrum of inviscid gravity-capillary surface waves. *J. Fluid Mech.* **83**, 737–739.

JÄHNE, B. & RIEMER, K. 1990 Two-dimensional wave number spectra of small scale water surface waves. *J. Geophys. Res.* **95**, 11531–11546.

KLINKE, J. & JÄHNE, B. 1992 2D wave number spectra of short wind waves-results from wind wave facilities and extrapolation to the ocean. In *Optics of the Air–Sea Interface: Theory and Measurements. Proc. SPIE 1749, Inst. Soc. Optical Engng*, pp. 1–13.

LONGUET-HIGGINS, M. S. 1963 The generation of capillary waves by steep gravity waves. *J. Fluid Mech.* **16**, 138–159.

LONGUET-HIGGINS, M. S. 1992 Capillary rollers and bores. *J. Fluid Mech.* **240**, 659–679.

LONGUET-HIGGINS, M. S. 1995 Parasitic capillary waves: a direct calculation. *J. Fluid Mech.* **301**, 79–107.

LONGUET-HIGGINS, M. S. & CLEAVER, R. P. 1994 Crest instability of gravity waves. Part 1. The almost-highest wave. *J. Fluid Mech.* **258**, 115–129.

LONGUET-HIGGINS, M. S., CLEAVER, R. P. & FOX, M. J. H. 1994 Crest instabilities of gravity waves. Part 2. Matching and asymptotic analysis. *J. Fluid Mech.* **259**, 333–344.

McGoldrick, L. F. 1965 Resonant interactions among capillary waves. *J. Fluid Mech.* **21**, 305–331.

Meiss, J. & Watson, K. 1978 Discussion of some weakly nonlinear systems in continuum mechanics. In *Topics in Nonlinear Dynamics* (ed. S. Jorna) *AIP Conf. Proc.* 46, pp. 296–323.

Milder, D. M. 1990 The effects of truncation on surface-wave Hamiltonians. *J. Fluid Mech.* **217**, 249–262.

Miles, J. 1957 On the generation of surface waves by shear flows. *J. Fluid Mech.* **3**, 185–204.

Miles, J. W. 1977 On Hamilton's principle for surface waves. *J. Fluid Mech.* **83**, 153–164.

Miller, S., Shemdin, O. & Longuet-Higgins, M. 1992 Laboratory measurements of modulation of short wave slopes by long surface waves. *J. Fluid Mech.* **233**, 389–404.

Perlin, M., Lin, H. & Ting, C.-L. 1993 On parastic capillary waves generated by steep gravity waves: an experimental investigation with spatial and temporal measurements. *J. Fluid Mech.* **255**, 597–620.

Press, P., Teukolsky, S., Vetterling, W. & Flannery, B. 1992 *Numerial Recipes in Fortran.* Cambridge University Press.

Valenzuela, G. & Liang, M. 1972 Nonlinear energy transfer in gravity-capillary wave spectra with applications. *J. Fluid Mech.* **54**, 507–520.

Watson, K. M. & McBride, J. B. 1993 Excitation of capillary waves by longer waves. *J. Fluid Mech.* **250**, 103–119.

Whitham, G. B. 1974 *Linear and Nonlinear Waves*, p. 530. John Wiley & Sons.

Wilton, J. R. 1915 On ripples. *Phil. Mag.* **29** (6), 688–700.

Zakharov, V. E. 1968 Stability of periodic waves of finite amplitude on the surface of deep fluid. *J. Appl. Mech. Tech Phys.* (English transl.) **2**, 190–194.

Zhang, X. 1995 Capillary–gravity and capillary waves generated in a wind wave tank: observations and theories. *J. Fluid Mech.* **289**, 51–82.

Zhang, X. & Cox, C. S. 1994 Measuring the two dimensional structure of a wavy water wave surface optically: a surface gradient detector. *Exps. Fluids* **17**, 225–237.